UNIVERSITÀ DEGLI STUDI DI PADOVA

Dipartimento di Ingegneria Industriale DII

Corso di Laurea Magistrale in Ingegneria Aerospaziale

Tesi di Laurea Magistrale

Ultrasonic vibration assisted turning for reducing tool wear in metal matrix composite machining

Relatore
Dott. Ing. Rachele Bertolini

Candidato
Edoardo Ghinatti
Matricola
1232108

Anno Accademico 2021-2022

Contents

List of Figures

List of Tables

List of Symbols

MMC	Metal Matrix Composite
PMMC	Particulate Metal Matrix Composite
V_c	Cutting speed
f	Feed
d	Depth of cut
MR	Material Removed
BUE	Built Up Edge
UTS	Ultimate Tensile Strength
CTE	Coefficent of thermal expansion
SiC	Silicon Carbide
TiC	Titanium Carbide
WC	Tungsten Carbide
TiAlN	Titanium Aluminium Nitride
AlN	Aluminium Nitride
BN	Boron Nitride
TiB	Titanium Boride
TiB_2	Titanium Diboride
Al_2O_3	Alumina
B_4C	Boron Carbide
PVD	Physical Vapor Deposition
CVD	Chemical Vapor Deposition
UVAT	Ultrasonic Vibration Assisted Turning
SEM	Scanning Electronic Microscope
EDS	Energy Dispersive X-ray Spectroscopy

Abstract

In automotive and aerospace industry there is a continuous research of materials with particular properties, as high specific strength, high specific stiffness, and wear resistance. Part of this research is focusing on particulate-metal-matrix-composites (PMMC), made of a metal matrix, as aluminium alloy or titanium alloy, and reinforcements which typically are hard particles, as silicon carbide SiC or titanium carbide TiC. The effects of reinforcements are an improvement of mechanical, thermal, chemical properties in respect of the monolithic alloys, but the same hard particles cause a severe tool wear, affecting machining time, costs of the tools, and final surface roughness. The purpose of this thesis is to study the tool wear during turning of an MMC, composed with a matrix of a series 3003-aluminium alloy, and a %30 in volume of SiC. A tungsten carbide tool with a physical vapor deposition coating of titanium aluminium nitride WC - PVD TiAlN was used, and the machining process was conducted with two techniques, conventional turning, and ultrasonic vibration assisted turning (UVAT), a technique to assist the machining process giving to the tool ultrasonic frequency vibrations. The machining procedure was made with a fixed depth of cut, three different feed rates, four different cutting speeds and two different machined volumes. After every machining process the flank wear was measured and was found that ultrasonic vibration assisted turning decreases the wear of the tool. In addition, it was made the analysis of the chips for every machining process.

Riassunto esteso

Nell'industria automobilistica e aerospaziale c'è una continua ricerca di materiali alto prestazionali, cioè con proprietà meccaniche elevate, ad esempio un'elevata tensione di snervamento specifica oppure un'elevata rigidezza specifica, o ancora un'elevata resistenza all'usura. Parte di questa ricerca si è concentrata nei materiali compositi a matrice metallica con rinforzi particellari (particulate-metal-matrix-composites (PMMC)) costituiti da una matrice tipicamente in lega di alluminio o di titanio, e dei rinforzi costituiti da particelle di materiali ad alta durezza, ad esempio il carburo di silicio SiC, il carburo di titanio TiC o in casi estremi polvere di diamante. È grazie a questi particolari rinforzi che un materiale tenero come una lega di alluminio può diventare sufficientemente prestazionale da competere con altre leghe più resistenti come gli acciai: infatti, l'effetto dei rinforzi può aumentare le caratteristiche meccaniche, termiche e chimiche della lega scelta. L'uso di questi rinforzi ha però un effetto collaterale importante, che ha limitato lo sviluppo di questi materiali innovativi: durante le lavorazioni di asportazione di truciolo, si genera un'elevata usura utensile che quindi costringe le industrie a usare utensili molto più performanti, ad esempio con inserti in diamante policristallino (PCD), e a limitare le velocità delle lavorazioni procurando un aumento dei tempi di lavorazione e soprattutto dei costi di produzione. Lo scopo di questa tesi è trovare un metodo per alleviare l'elevata usura durante la lavorazione di questi materiali, e in particolare ci si è concentrati sulla tornitura assistita ad ultrasuoni, che consiste nell'indurre l'utensile a vibrare ad una frequenza ultrasonica, cioè superiore ai 20 kHz. Il materiale composito analizzato in questa tesi è composto da una matrice di alluminio serie 3003, con all'interno il 30% in volume di carburo di silicio SiC, rientrante quindi nella categoria dei PMMC. Per le lavorazioni è stato scelto un utensile da tornitura in carburo di tungsteno con un rivestimento di nitruro di titanio e alluminio ottenuto tramite deposizione fisica da vapore WC - PVD TiAlN. Si sono scelti poi vari parametri di processo per capire qual è la condizione migliore per andare a lavorare questo tipo di materiale, in particolare quattro velocità di taglio, tre avanzamenti, due volumi di materiale asportato e una profondità di passata uguale per ogni esperimento. Le modalità di lavorazione sono state due: la tornitura assistita ad ultrasuoni, e la tornitura convenzionale, in modo da valutare direttamente l'effetto delle vibrazioni sull'usura utensile. Dopo ogni lavorazione,

si ha misurato l'usura del fianco dell'utensile, come spiegato dalla normativa, e si sono analizzati i trucioli. Alla fine delle misurazioni si ha scoperto che lavorare questo materiale usando la tornitura assistita ad ultrasuoni, con una velocità di taglio bassa e un avanzamento alto è la condizione migliore per limitare l'usura utensile.

Chapter 1

Introduction

The development of metal matrix composite (MMCs) in industry and research is increasing in recent years because of the enhanched properties that these materials can have in respect of alloys. For example, aluminium based MMCs can replace steel parts in automotive vehicles for example disc brakes, in which there is a big wear phenomena, because of the friction that these parts necessary must make to slow the wheels of cars, trucks, trains or planes. Another purposes are some peculiar parts of an engine: in fact, the wear rate, corrosion and fatigue subjected to the engine is one of the biggest problems in the mechanical industry, so it must be used a proper material which can resist this type of stresses. MMCs have some interest also in aerospace vehicles, for example tungsten based MMC are one of the few materials that can be used in nozzle inserts for rockets. The metal matrix composite have better mechanical properties than monolithic alloys but there is a main issue during the manufacturing process of the MMCs: in fact, there is a high wear rate of the tools during all the machining processes because of the hard reinforcements in the MMC which cause an high abrasion wear on tools cutting edge. So, industry is forced to use polycrystalline diamond tools (PCD) or cubic boron nitride (CBN) which are the hardest and expensive tools commercially avaiable, so there is a need of research for methods which can lower tool wear, in order to let the industry to use less expansive tools as tungsten carbide tools (WC). The lowering of wear rate will also affect the machining processes, increasing the quality of the surface roughness and also lowering the power used for machining. This thesis is focused on presenting a method to lower the wear on a WC tool during a turning process, using a technique to assist the cutting process: the ultrasonic vibration assisted turning. This method is compared with the conventional turning to understand the effect of ultrasonic vibration assisted turning in the process.

In chapter 2 there is a little introduction which describes generally the metal matrix composite materials: how to produce them, so casting and additive manufacturing; how to machine them; what type of matrix or reinforcements can be used and why they are so important for the industry.

In chapter 3 will be presented elements of machining theory to understand the main parameters used for turning.

In chapter 4 there is the characterization of the metal matrix composite analysed in this thesis, so it will be explained the procedure used to characterize it and the properties found after this analysis.

In chapter 5 there is the machining setup, in which it's explained how the sample was machined. In this chapter it's explained also why it was chosen the tool and also the cutting parameters. It's described also how the ultrasonic generator works and why it was used.

In chapter 6 there is the presentation of the data and the results obtained, and it will be explained also some non-intuitive results. There will be the conclusions of this work and suggest further research that can develop techniques for metal matrix composite machining.

Chapter 2

Overview of metal matrix composites

Metal matrix composites materials (MMC) are constituted by a metal or an alloy matrix and a mixture of reinforcements material to enhance the metal alloy properties [18]. Reinforcements can be divided in three main categories, as shown in figure 2.1: continuous fibers 2.1a, whiskers 2.1b or partice reinforcements 2.1c.

(a) Long or continuous fibers   (b) Whisker or short fibers   (c) Particellar
                                                                    reinforcements
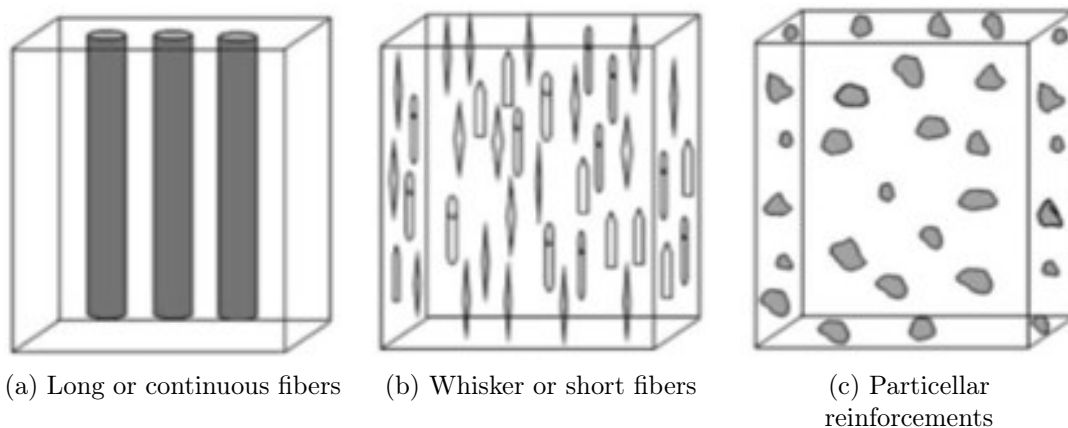
Figure 2.1: Types of reinforcements typically used in metal matrix composites.

The result of this combination is a material which has in general better properties than the individual components of the MMC. Another characteristic of these materals is the ease of changing properties, because it's enough to change a property of the constituents, for example the volume of reinforcements, shape of the reinforcements or the metal alloy, to have a significant change of global properties of the MMC.

Most of the metal matrix composites are made of an aluminum matrix, but also other metal alloys can be used, for example titanium alloys and magnesium alloys.

MMCs have enhanced properties than the bulk materials:

- higher specific strength σ/ρ and stiffness E/ρ;

3

Matrix alloy	Reinforcements	ρ [kg/m^3]	E [MPa]	σ_Y [MPa]	Reference
Al 2024	-	2600	236	220	[4]
Al 2024	5% SiC	2400	248	236	[4]
Al 2024	10% SiC	2300	265	257	[4]
Al 2014-T6	-	*2800*	476	429	[22]
Al 2014-T6	20% SiC	*3000*	508	457	[22]
Al 2014-T6	20% Al$_2$O$_3$	*3100*	515	495	[20]
Al 6061-T6	-	2710	290	275	[21]
Al 6061-T6	15% SiC	2770	340	290	[21]
Al 6061-T6	20% SiC	*2850*	410	345	[21]
Al 6061-T6	30% SiC	2910	435	380	[21]
Al 6061-T6	20% Al$_2$O$_3$	2700	349	307	[20]

Table 2.1: Main properties of metal matrix composite in function of reinforcements: *density ρ, Young's modulus E* and *yield stress σ_Y*. Values in *italic* are approximated. A more complete table of values can be found in [23].

- higher wear resistance and fatigue resistance;

- higher elevated-temperature properties;

- lower rate of creep (deformation caused by a constant force applied for a long time);

- lower coefficient of thermal expansion.

A table of values of the main mechanical properties of metal matrix composites with different reinforcements is shown in table 2.1.

MMCs have better properties than other composites, for example polymer matrix composites PMC, because they have better performance at high temperatures, fire resistance and low outgassing, which is a key property for aerospace purposes [5]. These materials have downsides: they are often expensive materials, for example titanium, and also they are particularly difficult to machine, because the reinforcements, which are much more harder than the monolitical alloy, could be also harder than the cutting tool itself so they cause an high abrasion wear and also a worsening of surface roughness in the final workpiece [16]. Despite this disadvantages, there is a strong interest of MMCs in industry, because of the special properties and characteristics, and so several applications can be covered. For example, military industries use MMC for balistics purpose, but also aerospace and automotive sector is starting to use more the MMCs, for the main purpose of lowering the weights of vehicles, which will cause a lowering of productions and mantainance costs, and a

decrease of pollution during both productions and usage of those products. Also, they can sustain a major fatigue load than the bulk material, and also have a major resisitance to impact, which can replace more brittle materials in automotive vehicles, for example pistons, piston rods or cylinder parts, which are the more important parts in a car engine [13]. MMCs have applications also in electronic sector, for the productions of microprocessors and other components, because of the excellent heat transfer properties. New type of superconductors can be made also with the metal matrix composite [8]. One of the most used types of MMC are particulate-based metal matrix composites (PMMCs), because in these materials the reinforcements are evenly distributed so they can be considered isotropic and homogeneous materials.

2.1 Matrix alloys

MMCs have a matrix which is usually a metal alloy, the use of pure metals as the AA1xxx series is rare, because of the peculiar purposes of this materials.

2.1.1 Aluminium alloy matrix

Aluminium alloys are the most used material in the industry of metal matrix composites because of its low density, which permit the replacement of steel and the development of lighter products. Also, aluminium has one of the highest electrical conductivity in nature, second only to silver and copper. It's also a non-ferromagnetic element, which permit to be compatible with electric circuits, and they are often used for high-voltage cables, coils for high-power transformers and for grounded domestic appliances casings. They can be used both wrought or casted alloys, and the most used alloys are the heat-treatable alloys: wrought alloys 2xxx series, 6xxx, 7xxx or the equivalent casted alloys 2xx, 3xx and 7xx [7].

The reinforcements typically used with aluminium alloy matrices are silicon carbide SiC, alumina Al_2O_3, boron carbide B_4C, aluminium nitride AlN and boron nitride BN [13].

2.1.2 Titanium alloy matrix

Titanium and titanium alloys are used because of the high specific stiffness and high specific ultimate tensile strength UTS, high corrosion resistance, fatigue resistance, high crack resistance and creep resistance, as described in [10]. The most used titanium alloy is the Ti6Al4V because it has the best properties among titanium alloys [18]. Because of those properties, it's often used in aeronautics and automotive industry, but also for biomedical purposes: in fact, titanium is biocompatible

so it can be used for implants [9]. The reinforcements used can be titanium-based ceramics, as TiB, TiB_2, TiC but also other ceramics as SiC or Al_2O_3.

2.1.3 Magnesium alloy matrix

MMCs based on magnesium alloys have a lower density than aluminium, which imply that have a potential development on aerospace industry where there is always a constant need of lighter structures. They are used often in automotive industry for example as disk rotors and gears, but they can be used also for biomedical purposes, for example implants. Their side effect is that they have high production costs because of their special manufacturing process. Also, an heat treatment can't be useful because it doesn't improve the mechanical properties of the alloy. The most used magnesium alloy in automotive industry is AM60 and AZ91 which are magnesium-aluminium alloys. The reinforcements used with magnesium alloys are ceramics, and the best choice for these alloys is silicon carbide SiC which has the higher wettability and also the best stability with melted magnesium [13].

2.1.4 Copper alloy matrix

Copper alloys are not used for aerospace purposes because of their high density and costs. If it's reinforced with alumina Al_2O_3 they can be achieved higher thermal and electrical conductivity, higher strength and resistance to annealing, which makes these materials suitable for electric purposes. It can be done also a combination of copper and silicon carbide SiC in order to have a lower coefficient of thermal expansion CTE, but it's difficult to produce this MMC because of high affinity between SiC and copper at high temperatures which create reactions and products that increase the CTE [13]. Also, a special case of copper MMCs has reinforcements of niobium-titanium Nb−Ti and niobium-tin Nb−Sn to create type II superconductors used for supermagnets.

2.1.5 Other alloys

- Super alloys: they are used for particularly mechanically and thermically stressed parts of machines such gas turbine blades for airplanes or gas-fired power plants [13].

- Cemented carbides: it's a particular case of MMC which are often used for tools production. The most famous cemented carbide is formed by a matrix of cobalt (5 to 25%) and reinforcements of tungsten carbide WC[1] (75 to 95%).

---

[1]It's commercially know as Widia

- *Cermets*: often used for electrical and electronic puroposes, they are made of a ceramic part as reinforcement and a metal part as binder. The ceramic part can be an oxide, such as alumina Al_2O_3, a boride such as TiB_2 or a carbide such as TiC, while the metal part can be nichel, molybdenum or cobalt.

2.2 Production of metal matrix properties

Here it's described the main methods to produce particulate MMCs in industry. There are two main categories of methods: *liquid state processing* and *solid state processing*.

2.2.1 Powder blending

Powder blending is one of the most used *solid state processing*, and it's used for relatively small workpieces, as cutting tools or engine parts, or for high melting point alloys or metals, for example tungsten. If possible, the metal alloy is melted and then injected in a small orifice, which generates a thin jet. Then, the jet is broken by multiples high pressure air jets which then can create an alloy powder. This powder will become the metal matrix of the final MMC, and it's well understandable that this process will create irregular metal shapes and not perfect spherical particles, which can lead to a worsening of the final result. After this process, the metal powder is mixed with the particles of the reinforcement, and it can be done in dry conditions (mechanical mixture) or using a third material which can be a binder, a lubricant to permit the perfect flow thorugh the particles, or an additive to facilitate sintering. After blending, the mixture is subjected by a process of high-pressure compaction which creates the *green compact* between (typically) two dies, which gives to the piece the near-net-shape and guarantee the contact between the particles. After that, a *sintering* process is needed to permit to the particles to bind together and become a whole piece: the green compact is heated to a temperature below the melting point of the metal, but high enough to allow bonding between particles [18].

2.2.2 Stir casting

Stir casting is one of the most used liquid state processing, and it's used for relatively large workpieces or production, as disc brakes for heavy automotive purposes. It can be done only with metal alloys which have a low melting point, for example aluminium. In this process, the metal is placed in a die and then melted. Then the alloy is mixed with a rotating blade, and during this process the particulate reinforcements, which are pre-heated to let a better bonding, are inserted directly into the vortex of molten alloy. The maximum volume of particles that can be

incorporated in the melted alloy is 30% because higher values creates clusters and sediments which can lead to a non-uniform MMC. A problem arises during the stir casting process, as the reinforcements are not uniformly distributed and form sediments in the molten alloy [25].

2.3   Machining processes for metal matrix composites

In both the manufacturing process of MMCs and metal alloys there is the machining step, and this is necessary to have the final surface roughness and dimensions computed in the design process. Because of hard reinforcements, it's necessary to use tools which can withstand the high abrasion wear generated by MMCs, so it's necessary to use the hardest tools commercialy avaiable, for example polycristalline diamond tools (PCD) or cubic boron nitride (CBN). Ceramic tools are less used in industry than CBN and PCD tools, but they can be used at low cutting speed. Tungsten carbide tools (WC) are the tools with lowest hardness, so they are rarely used because of the high abrasion wear given by the reinforcements.

In [1] a set of different tools, PCD tools, CBN tools and WC tools, it's used in order to study the tool wear, surface roughness and forces during turning and milling of a titanium-based MMC, with different cutting parameters. The WC tools present high wear in a condition of high cutting speed $V_c = 80\,\text{m}\,\text{min}^{-1}$, high feed $f = 0{,}35\,\text{mm}\,\text{rev}^{-1}$ and high depth of cut $d = 0{,}2\,\text{mm}\,\text{rev}^{-1}$, while the lower wear is obtained at low speed $V_c = 40\,\text{m}\,\text{min}^{-1}$, low feed $f = 0{,}15\,\text{mm}\,\text{rev}^{-1}$ and high depth of cut $d = 0{,}2\,\text{mm}\,\text{rev}^{-1}$, or at lower speed $V_c = 60\,\text{m}\,\text{min}^{-1}$, high feed $f = 0{,}35\,\text{mm}\,\text{rev}^{-1}$ and low depth of cut $d = 0{,}1\,\text{mm}\,\text{rev}^{-1}$, implying that *wear on WC tools decreases when feed and depth of cut are inversely proportional*, in order to have a constant cutting area. CBN tools present high wear in a condition of high cutting speed $V_c = 200\,\text{m}\,\text{min}^{-1}$, low feed $f = 0{,}35\,\text{mm}\,\text{rev}^{-1}$ and high depth of cut $d = 0{,}2\,\text{mm}\,\text{rev}^{-1}$, while the lower wear is obtained at low speed $V_c = 150\,\text{m}\,\text{min}^{-1}$, low feed $f = 0{,}3\,\text{mm}\,\text{rev}^{-1}$ and low depth of cut $d = 0{,}1\,\text{mm}\,\text{rev}^{-1}$, or at higher speed $V_c = 175\,\text{m}\,\text{min}^{-1}$, high feed $f = 0{,}6\,\text{mm}\,\text{rev}^{-1}$ and low depth of cut $d = 0{,}1\,\text{mm}\,\text{rev}^{-1}$, so *the cutting area $A_C = f \cdot d$ must be set at low values, while the cutting speed can be high*. It must be noticed that the cutting parameters used for CBN tools are significantly higher than parameters during WC, because of their strength against abrasion. PCD tools present high wear in a condition of high cutting speed $V_c = 500\,\text{m}\,\text{min}^{-1}$, high feed $f = 0{,}5\,\text{mm}\,\text{rev}^{-1}$ and high depth of cut $d = 0{,}15\,\text{mm}\,\text{rev}^{-1}$, while the lower wear is obtained at lower speed $V_c = 450\,\text{m}\,\text{min}^{-1}$, high feed $f = 0{,}5\,\text{mm}\,\text{rev}^{-1}$ and low depth of cut $d = 0{,}1\,\text{mm}\,\text{rev}^{-1}$. In the end, it can be said that to limit the tool wear it's necessary to set a *medium-low cutting speed*, *high feed* and *low depth of cut*, because in this case the tool will travel a *low cutting distance* so the abrasion effect due to the reinforcements will

be low. The main wear mechanism on CBN and WC is abrasion, while on PCD it's chipping because of the high hardness of those tools, so it's important to consider that there could be chipping on PCD inserts which can cause *catastrophic failure* and could irreparably ruin the final workpiece, as described in [24].

In [3] it's analysed the tool wear of WC, PCD and monocrystalline diamond MCD tools during machining of a aluminium-based MMCs, and it's found that there WC tools can't withstand very high cutting speeds as $V_c = 200\,\mathrm{m\,min^{-1}}$ because of high flank and crater wear that shortens the tool life on WC tools in seconds, while PCD and MCD tools not only can resist to the higher speed but also during machining there is a development of a built up edge-BUE which protects the tool tip.

In [2] it's analysed the effect of UVAT and cooling with Minimum Quantity Lubrication (MQL) during machining of aluminium based MMCs, and the tools used are a WC tool and a PCD tool. All experiments were taken with fixed speed, feed and depth of cut. It's found that during UVAT the temperature increases because of vibrational energy transmitted to the workpiece. In terms of wear, the WC tool has the lowest value of wear during UVAT, while the PCD tool has no appreciable wear in every case because of the low cutting speeds used for machining.

In the end, it can be said that :

- PCD tools can resist to the high abrasion wear due to reinforcements of MMCs, so they can be used for turning at high cutting speeds, but can be subjected to chipping which can result to catastrophic failure; they are probably the only tools that can be used for finishing operations, because the high hardness permit both a *small nose radius* and *the abrasion resistance* required for MMC machining.

- CBN tools have less resistance than the PCD tools so they must be used at lower cutting speed than PCD;

- WC tools must be used at very low cutting speed because they can't withstand the abrasion wear of the MMCs, but if it's used a high feed and low depth of cut they can resist to the high wear because of the lower cutting distance which lower the number of contacts with particle reinforcements. On the other hand, WC tools can't withstand finishing operations of MMC because of the high abrasion wear of the MMC reinforcements.

- It can be used also UVAT to decrease the wear effect because of the softening of the matrix due to the increase of temperature.

- The combination of WC tools and UVAT can be used only in roughing operations because the induced vibration can cause an uneven surface which affects general surface roughness, as explained in subsection 3.3.4.

9

Chapter 3

Elements of machining theory

3.1 Mechanism of chip formation

In every machining operation there are two main parts: the *workpiece*, which is unprocessed material that will become a final product, and the *tool* which will remove the material from the net-shape workpiece. The material removed from the workpiece is called *chip*.

Every tool has three main surfaces which are enlightened in 3.1a and figure 3.2:

- *rake face*: it's the surface facing directly the workpiece, and it's where the chip will flow;

- *flank face*: it's the surface facing the machined part of the workpiece;

- *cutting edge*: it's between the rake face and the flank face, and it's the most important side of the tool because it touches directly the workpiece and causes the cutting mechanism.

The angle between the rake face and the surface of the workpiece is the *rake angle* α, which can affect the flow of the chip and also the forces on the tool, changing the power consumption of the machining process, surface roughness and stresses in the cut. Between the flank and the workpiece there is the *clearance angle* ζ, which must be greter than zero to not have a plowing effect on the workpiece. Between the flank face and the rake face there is the *tool angle* λ. Rake angle α, clearance angle ζ and tool angle λ are the three main angles which affects directly the machining operation and must be chosen carefully to permit a correct machining.

3.1.1 Orthogonal cutting

The main theory used for modeling cutting mechanism of machining operations is orthogonal cutting [18]. The main hypothesis are:

11
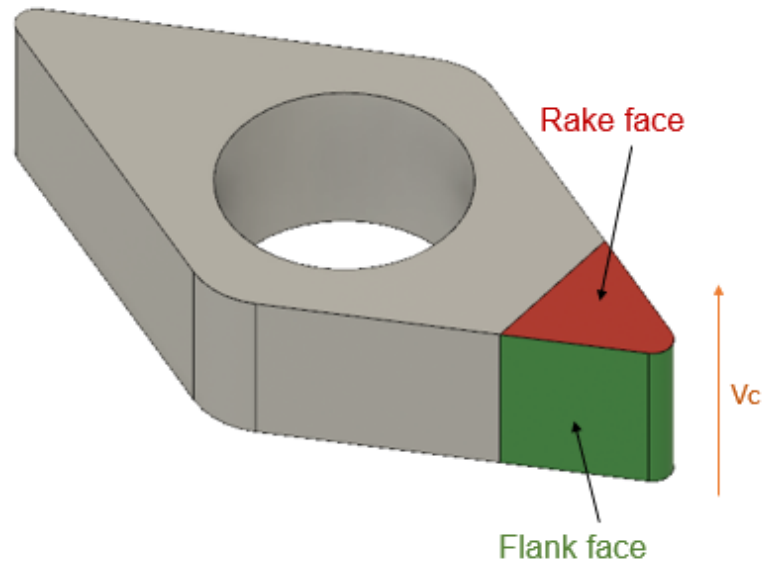
(a) Main faces on a tool
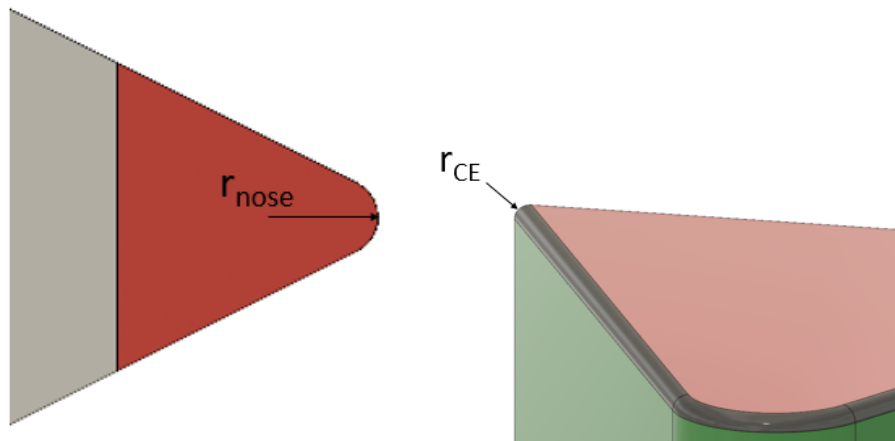
(b) Nose radius of a tool   (c) Cutting edge radius in a tool

Figure 3.1: Hypothetical tool for turning.

- The tool is perfectly sharp, so the radius of the cutting edge is infinitesimal $r_{tool} \to 0$; in a real tool there is a little curvature as shown in 3.1c;

- All of the cutting phenomena is resctricted to a 2D behaviour, so all the mechanism can be modeled in a plane, as shown in 3.2;

- A direct effect of the previous condition is that the chip doesn't flow to the side, it flows only along the rake face;

- The tool cuts and contacts the workpiece only in the rake face;

- Cutting edge is perpendicular to the cutting direction;

- There is only one main deformation that occours adiacent to the shear plane.
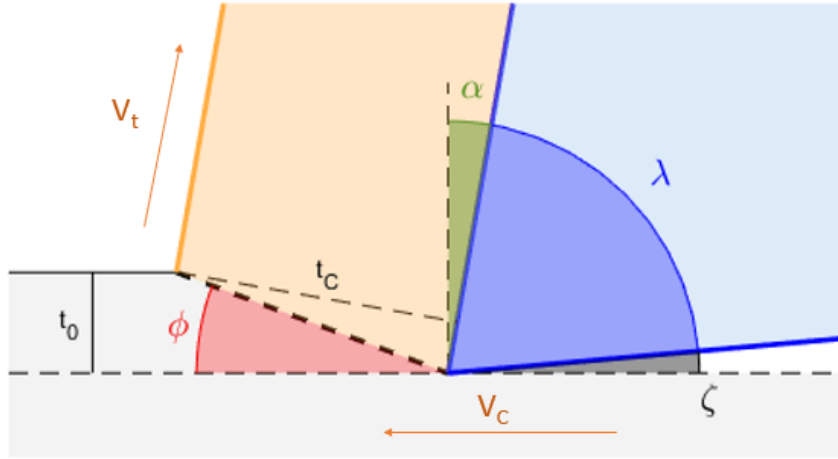
Figure 3.2: Cinematics of chip formation: the gray area is the workpiece, the blue part is the tool, the orange part is the chip. They are shown the cutting speed V_C, the depth of cut t_0, the rake angle α, the clearance angle ζ, the tool angle λ, and the chip thickness t_C from which can be computed the shear angle ϕ and defined the shear plane (thick dotted line).

The main cutting parameters that occours during machining are cutting speed V_C and depth of cut t_0, while the parameters of the tool are rake angle α, tool angle λ and clearance angle ζ. These parameters are given from the operator and so they are known before the cut and fixed. There is another parameter which can't be known before the cut which is the chip thickness t_C, and so it must be measured after the cut. From these dimensions it can be computed the cutting ratio r, and after that it can be found the *shear plane* where the primary (and only, in this theory) deformation takes place. The inclination between the shear plane and the uncut workpiece is given by the shear angle ϕ, computed in the Equation 3.2.

$$r = \frac{t_0}{t_C} \tag{3.1}$$

$$\tan \phi = \frac{r \cdot \cos \alpha}{1 - r \cdot \sin \alpha} \tag{3.2}$$

13

3.2 Turning operation theory

Machining theory can be applied for all the types of machining operations and of course it can be applied for the turning operation. Turning is a machining process in which the workpiece is fixed between three or four *cluckes*, and then rotated by a *spindle*. During this rotation, which can be at fixed speed (conventional turning) or variable speed (complex cut), a tool approaches to the material and starts cutting, as shown in figure 3.3.

The main cutting parameters are:

- *Cutting speed V_C* [m/min]: it's the relative speed between the tool and the workpiece. This parameter is directly proportional to the rotation speed N [rev/min] of the spindle;

- *Feed f* [mm/rev]: it's the distance per revolution traveled by the tool in the direction given by the axis rotation. This parameter is directly proportional to the feed rate v_f [mm/min];

- *Depth of cut d* [mm]: amount of material removed, measured in radial direction (perpendicular to rotation axis);

The main geometric parameters during are:

- External diameter[1] of the workpiece D_0 [mm];

- Final diameter D_f [mm];

- Length of the workpiece L_{cut} [mm];

The orthogonal cutting theory explained in subsection 3.1.1 have a direct conversion of parameters in turning as shown in figure 3.4.

From this setup can be easily computed the following parameters:

Mean diameter during one cut:

$$D = \frac{D_0 + D_f}{2} \quad [\text{mm}] \tag{3.3}$$

Cutting speed

$$V_c = \pi D N \quad [\text{m/min}] \tag{3.4}$$

Depth of cut

$$d = \frac{D_0 - D_f}{2} \quad [\text{mm}] \tag{3.5}$$

---

[1]This is true for external turning only: there are also similar operations as *internal turning* in which the initial diameter is the inner diameter.
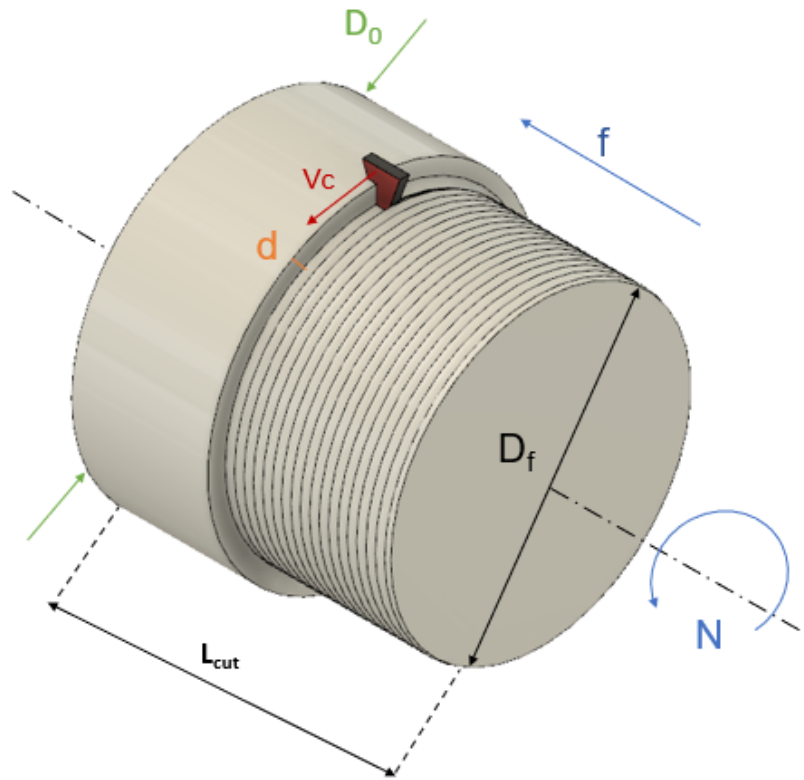
Figure 3.3: Turning parameters: feed f (blue), cutting speed V_c (red), depth of cut d (orange), rotation speed N (blue). Geometric parameters: External diameter D_0, final diameter D_f, length of the workpiece L_{cut}.

Feed rate

$$v_f = \frac{f \cdot N}{1000} \quad [\,\mathrm{m/min}\,] \tag{3.6}$$

Material removal rate: volume of machined material per minute

$$MRR = V_c \cdot d \cdot f \quad [\,\mathrm{m^3/min}\,] \tag{3.7}$$

Turning time: time necessary for one cut

$$t_{cut} = \frac{L_{cut}}{fN} \quad [\,\mathrm{min}\,] \tag{3.8}$$

Final roughness:

$$R_t = \frac{f^2}{8R_{tool-nose}} \quad [\,\mathrm{\mu m}\,] \tag{3.9}$$

15
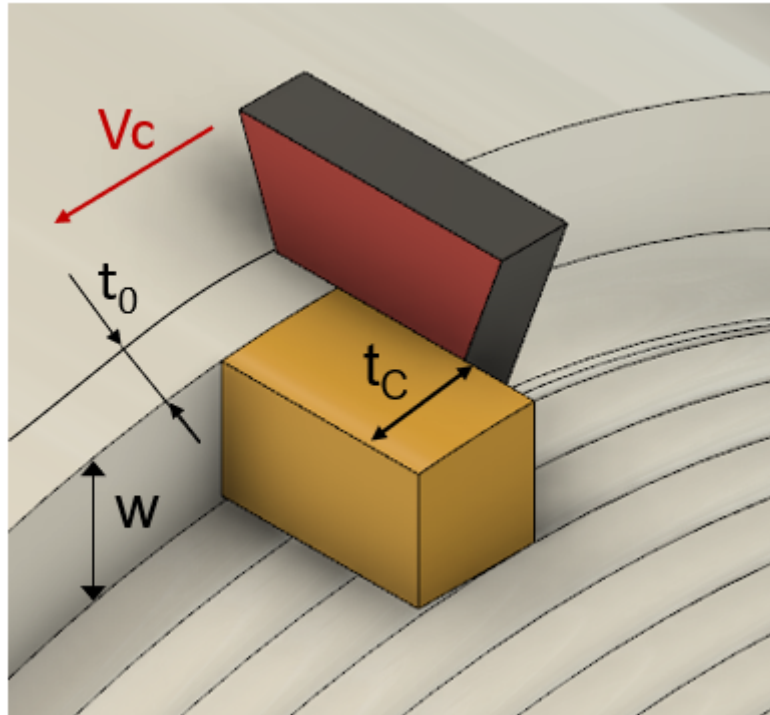
Figure 3.4: Machining parameters of the orthogonal cutting in turning: cutting speed is the same of the orthogonal cutting; feed is the depth of cut of orthogonal cutting $f = t_0$; depth of cut is the width of cut of orthogonal cutting $w = d$.

3.3   Tool wear

During machining operations tool wear occours naturally because of many issues: abrasive effect of the workpiece grains, increase of temperature of the workpiece, plastic deformation on the tool tip or chemical affinity with the workpiece/lubricant. These effects change the theoretical behaviour of every cutting operation, and can cause a worsening of the final surface roughness, an increase of the cutting forces, a generation of vibrations, so in the end the final dimensional tolerances can't be mainteined, ruining the workpiece (which could be expensive) and also the lathe can be damaged, causing an inevitable increase of time and costs in the production system. In order to avoid these consequences it must be used a model to determine the maximum life of the tool in machining process.

3.3.1   Models for tool wear

The tool life can be computed with the *Taylor's equation*:

$$V_c T^n = C \qquad (3.10)$$

16

V_c is the cutting speed, T is the life of the tool in minutes, C is the cutting speed corresponding to a tool life of $1\,\text{min}$, and n is a constant. The main hyphotesis of this equation is that cutting speed is the main parameter that affects the tool wear, because of the increase of temperature caused by friction between tool and workpiece. C and n are computed by doing experimental trials with at least five different speeds, and then doing a best-fit approximation, according to the ISO 3685 [24].

This equation can be further expanded to the other cutting parameters, depth of cut d and feed f:

$$V_c T^n f^x d^y = C \tag{3.11}$$

obtaining a hyper-surface which describes the wear of the tool in function of the three cutting parameters.

3.3.2 Types of tool wear

Tool wear is a complex phenomena which can affect the tool in many zones with many behaviours, making the measurement of tool wear and the computation of tool life a complex problem, so it must be chosen a *tool life criteria*, to define which type of wear must be measured. The most common types of tool wear are, according to the ISO 3685 [24]:

- *Flank wear*: It's the most common type of wear, and it's also the best known. It affects the flank plane of the tool and it depends obviously on the materials of workpiece and tool, but in particular on the presence of hard particles or grains in the workpiece. An example of flank wear is shown in figure 3.5, which can be noticed the *flank wear area*. From the measurement of the flank wear area it can be computed the *mean flank wear* Vb_{mean} and also the *major flank wear* Vb_{max}. It can be seen that the Vb_{max} takes place near the tip of the tool because it's the point at the highest temperature, so where wear mechanism is at the maximum.

- *Crater wear*: it's the most common type of wear which affects the rake face of the tool. It causes a little pit characterized by the *maximum crater depth KT*.

- *Notch wear*: is a particular case of flank wear and face wear combined. It takes place in the end of the flank wear area, so it's easily recognizable because the Vb_{max} takes place near the tip, as explained above.

- *Chipping*: a portion of the tool tip is removed in one take, breaking the cutting edge and changing the form of the tool. It's caused by a combination of brittle tool material, thermal cracking and variable mechanical loads which are caused by heterogeneous materials or interrupted cuts. An example of
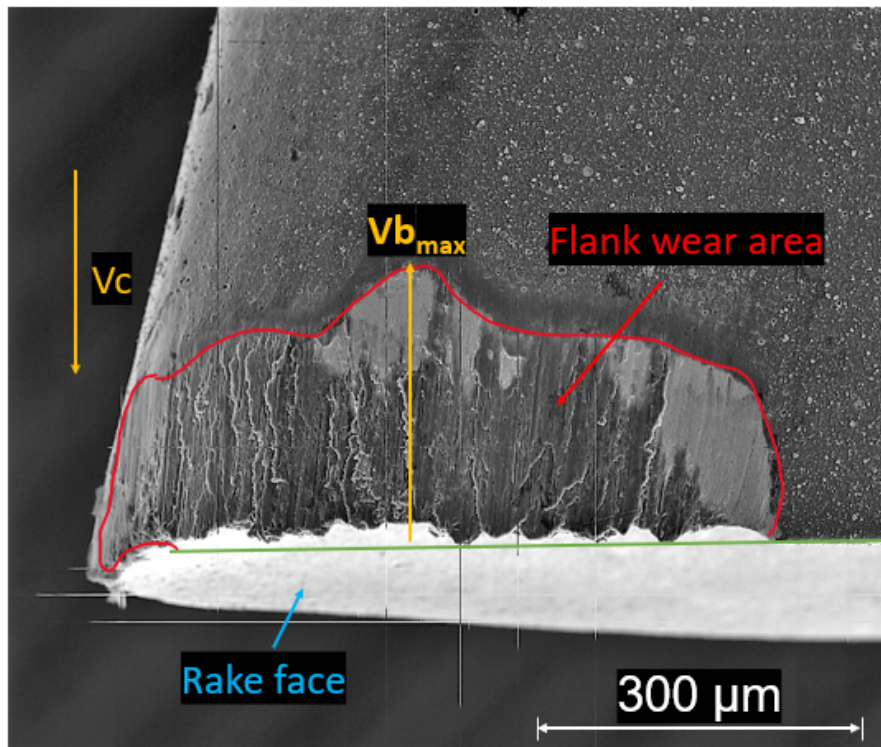
Figure 3.5: Example of flank wear: the red area is the flank wear area and the yellow arrow is the Vb_{max}.

chipping is shown in figure 3.6. It must be explained that chipping can cause the tool to be round enough to cause ploghing on the workpiece, so the tool doesn't cut anymore, causes residual stresses on the workpiece due to compression of ploughing effect.

ISO 3685 [24] it's the standard norm which explain how to study the wear on tools and how to quantify the life of tools. From the ISO 3685, if the main wear mechanism is located in the flank, the tool life criteria can be:

$$Vb_{mean} = 0{,}3 \, \text{mm} \qquad or \qquad Vb_{max} = 0{,}6 \, \text{mm} \qquad (3.12)$$

If the main wear is caused by the chipping of the tool, the tool life criteria must be:

$$Vb_{max} = 0{,}6 \, \text{mm} \qquad (3.13)$$

3.3.3 Most used tool materials

As explained above, the choice of the tools is fundamental for having successful cutting operations, in which for example it's obtained the surface roughness, or

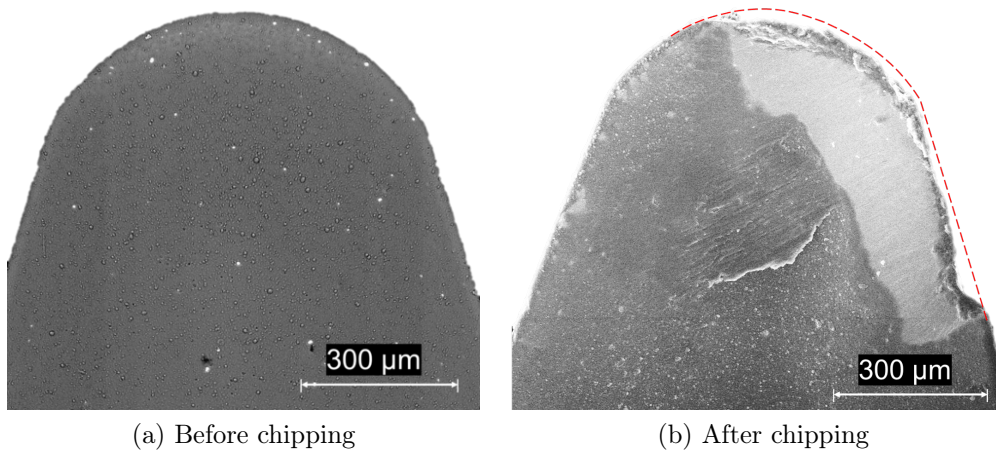(a) Before chipping   (b) After chipping

Figure 3.6: Example of chipping: the red dotted line traces the original shape of the tool.

to prevent the workpiece to be ruined. The tool must also resist to the wear mechanisms which are always present in cutting operations. In order to have these properties, the tool must be enough hard to resist flank wear and deformation of the tip, tough to prevent the breakage which can cause catastrophic failure, resistant to thermal changes, chemically stable to prevent oxidation which can ruin the tool itself and non reactive with the workpiece to impede the diffusion of tool material which can affect both tool and workpiece.

Here are exposed a list of most common materials used for tools:

- *Cemented carbide*: it's a metal material composite which is composed by particles of tungsten carbide WC placed in a metallic matrix, for example cobalt. This composition is necessary because WC is a hard but brittle material, so to have a tougher tool it's necessary to add a small percentage of cobalt, for example %6 Co. It's product by sintering and then sharpened with silicon carbide SiC or other harder materials. Another important parameter for these tools is also the WC grain size: at fine grain size, the hardness is at maximum, as described by the Hall's Petch equation:

$$\sigma = \sigma_0 + \frac{k_Y}{\sqrt{d}} \tag{3.14}$$

where σ is the yield stress, d is the mean diameter of the particles, k_Y and σ_0 are constants depending on material. Another type of cemented carbide is called *cermet*, and typically it's a combination of a titanium-based hard particles placed in tungsten and cobalt a matrix. Both of these materials are designed to be self-sharpening and wear resistant, to guarantee an high tool life and low surface roughness.

19

- *Ceramics*: they have generally a high wear resistance, so they can cut at high cutting speed. The most used materials are: aluminia particles Al_2O_3 sintered with zirconia ZnO_2 or titanium carbides TiC or SiC whiskers; Silicon nitride ceramics Si_3N_4 used for grey cast iron; SiAlON used for heat resistant super alloys.

- *Polycrystalline cubic boron nitride* CBN: it's a material which maintains its hardness also at high temperature, so it can be used to cut *difficult to cut materials* at high cutting speeds. It's the only material which can resist a finishing operation for the hardened steels.

- *Polycrystalline diamond* PCD: it's a metal matrix composite with diamond particles sintered with a metallic matrix. Diamond is the hardest material avaiable in industry, and it can be used for example for sharpening of CBN, ceramic or cermet tools. It's also the most abrasion resistant material, so it's suitable for machining *difficult to cut materials*. It can't be used for every machining operation: in fact, it can't be used for machining steels because carbon is soluble in iron, causing the dissolution of the tool in the workpiece [18].

During machining it's easy to find some workpiece materials which have an external thin layer harder than the rest of the material, and this is caused for example by oxidation (rust on steel), or residual stresses caused by previous manufacturing. Also, there might be a machining process which is not compatible with the hardest tools, for example because the material is heterogeneous and it causes some variable loads and vibration which can damage the tool. To prevent this, it can be used a tool with a special coating, which can be wear-resistant or chemically stable. There are two main methods to produce a coating on a tool: *Chemical Vapor Deposition* CVD or *Physical Vapor Deposition* PVD.

- Chemical Vapor Deposition is an *additive manufacturing process*: consist of a deposition of hard particles which has to react with the tool material, and it's done at a temperature of $T_{CVD} = 700\,°C$. The most used material for this purpose is titanium nitride TiN or alumina Al_2O_3 and it's done on cemented carbides tools.

- Physical Vapor Deposition is another additive manufacturing process which works at a lower temperature, $T_{PVD} = 400\,°C$, and consist of a evaporation of a metal which reacts with the nitrogen in the air, which then adhere on the tool forming an hard coating. The most used material for this purpose is TiN and also the variants Ti(C,N) and (Ti,Al)N. Noteworthy is the latter, the titanium aluminium nitride, because is the hardest of the coatings and so it has an high wear resistance.

3.3.4   Assisted machining techniques

For particular materials or forms the conventional machining can't be used, so it's necessary to use some methods or techniques to assist the machining operation.

- *Lubricants*: they are often used during machining processes because they lower the temperature between the tools and workpiece interfaces and also decrease the friction, lowering the forces. The combination of these two effects lowers tool wear and permit a good surface roughness. The main lubricants and cooling used are typically a mixture of oil and water, but for enviromental regulations there is an increasing of research in the use of high-pressured air, but also cryogenic cooling is developing for materials as titanium, which has low thermal conductivity which causes an high temperature on the tool [18].

- *Ultrasonic vibration assisted turning* (UVAT): It's a technique in which the tool is subjected to a controlled high-frequency vibration. It works with a oscillating system, where the main component is an ultrasonic transucer that transform electric energy at a given frequency to mechanical energy at the same frequency. In ultrasonic vibration assisted turning the energy of vibrations is transmitted from the tool to the workpiece causing a local increase of temperature, as explained in [2]. This machining process can be used for lowering the flank wear, but it can be done only in case of roughing, because of the vibrations that cause a non-constant value of depth of cut, as shown in figure 3.7. This method can be used also to have a certain texture on a surface [12] or to weld low melting temperature material, for example plastics or aluminium [15].

- *Laser assisted machining*: an high density energy beam is used for increase the temperature of the workpiece locally, in order to lower the strength of the material [19]. This method lowers the forces on the tool decreasing the tool wear, but there must be also the awareness of the increasing of forces with cutting speed in hot conditions, because of the increase of deformation rate. The main side effect that must taken into account is that it creates local high deformations because of the increase of temperature, which can cause local damages on the machined surfaces.

- *Abrasive waterjet*: in this operation the workpiece is cut by a high pressure water jet mixed with small hard particles. The main property of this technique is that it has a low thermal effect so it avoids thermal cracking on the machined surface, and also it has a high material removal rate. It can be used for roughing of *difficult to cut materials* and also materials with low thermal conductivity [19].

- *Electro-discarge machining*: it's a method which erodes the workpiece by using a series of spark discarges generated by a sharp tool called electrode [19].
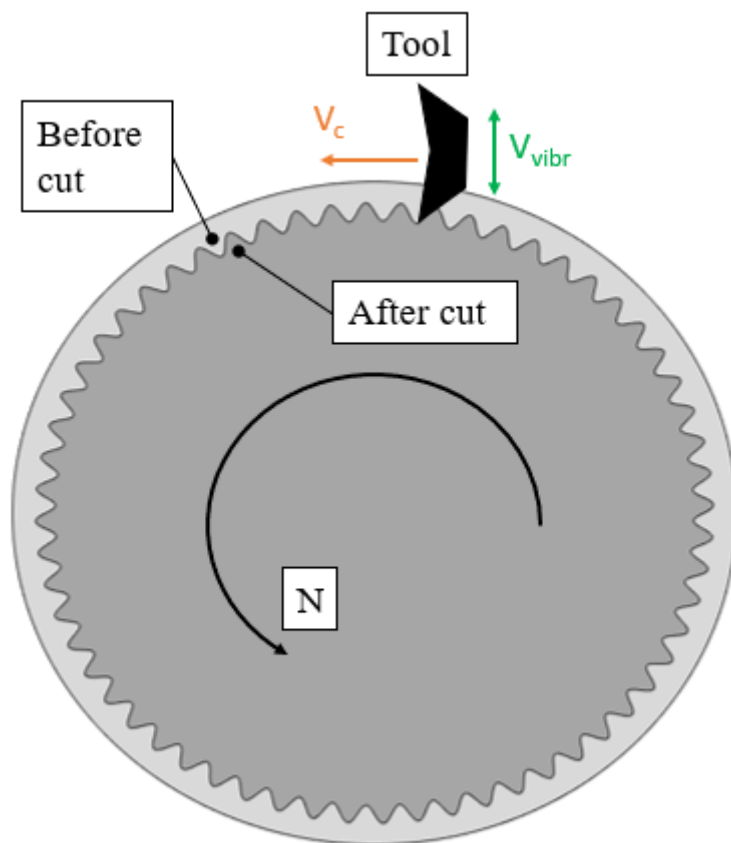
Figure 3.7: Effect of ultrasonic vibration assisted turning: the vibration causes an uneven surface in the workpiece

Chapter 4

Characterization of the MMC

4.1   Mechanical and thermical properties

The sample used in this thesis is a brake disc for heavy automotive purposes.It was given also the chemical composition of the MMC, explained in table 4.2 and also the type of aluminium alloy used in this MMC, which is commercialy known as a A359.0 casted alloy, equivalent to a series 3000 aluminium alloy. Mechanical and thermal parameters of the sample are explained in table 4.1: it can be enlighted that the Young's modulus in the MMC is much more higher than the Young's modulus of the monolithic alloy, so it demonstrates that reinforcements cause an improvement of mechanical properties.

Property		Al-3000	Al-MMC
Density	$[\,\mathrm{kg/m^3}]$	2560	2710
Young modulus	$[\,\mathrm{GPa}]$	69,1	108
Yield stress	$[\,\mathrm{GPa}]$	131	138,7
Ultimate stress	$[\,\mathrm{GPa}]$	181	178,3
Thermal expansion coefficient	$[\,\mathrm{\mu m/mK}]$	23,7	17,5
Specific heat capacity	$[\,\mathrm{J/kgK}]$	893	806
Thermal conductivity	$[\,\mathrm{W/mK}]$	166	168
Poisson's ratio	$[/]$	0,34	0,31

Table 4.1: Main properties of the monolithic aluminium alloy and the metal matrix composite

Element	C	Si	Mn	P	Cr	Ni	Ti	Cu	Sn	V
Wt%	6	20	0,01	0,003	0,0015	0,005	0,05	0,005	0,006	0,016
Element	Li	B	Pb	Fe	O	Zn	Mg	H	Na	Ga
Wt%	0,001	0,032	0,021	0,13	0,057	0,007	0,59	0,001	0,009	0,014

Table 4.2: Composition of the metal matrix composite, aluminium balances.

4.1.1 Production of the MMC

The method for producing tthe sample was *stir casting*: the aluminium alloy was melted and then mixed up with the SiC powder. Then the mix was cooled in a cylindrical mold in order to have a billet. After that, an open forging process and then other successive closed forging processes were done to get the near-net-shape. At this point, in order to have the final disc brake, some machining operation must be made, for example turning, milling and drilling, to have the final product with the requirements of size and surface roughness designed form the company. The sample used was not machined, it was forged in a intermediate step.

4.1.2 Preparation of the sample

The disc was not compatible with the CNC machine used for this thesis so a water-jet cut was necessary to do: in fact, only a water-jet cutting could be able to cut the sample material without changing the surface properties, where a laser cutting or a conventional saw could fail. This cut was done in order to have three pieces, shown in figure 4.1: the inner part 4.1a was used for the machining trials, the external part 4.1d were used for the characterization of the MMC and the inner part 4.1c was unitilized.

4.2 Procedure for the characterization of MMC

From the external part of the disc brake 4.1d were cut three pieces with dimension of $1\,cm^3$, to permit the characterization process.

4.2.1 Cold mounting

The samples were put in a die and then filled with two-component epoxy resin. After waiting one day to permit the complete reticulation process of the resin, it was removed from the die, obtaining a cilindrical shape with the incorporated samples, which had one side free each. The samples incorporated are shown in figure 4.2. This incorporation process was necessary in order to have a solid shape which was easier to handle and also to permit the same polishing process to each sample. A

(a) Inner part of the sample

(b) Whole sample

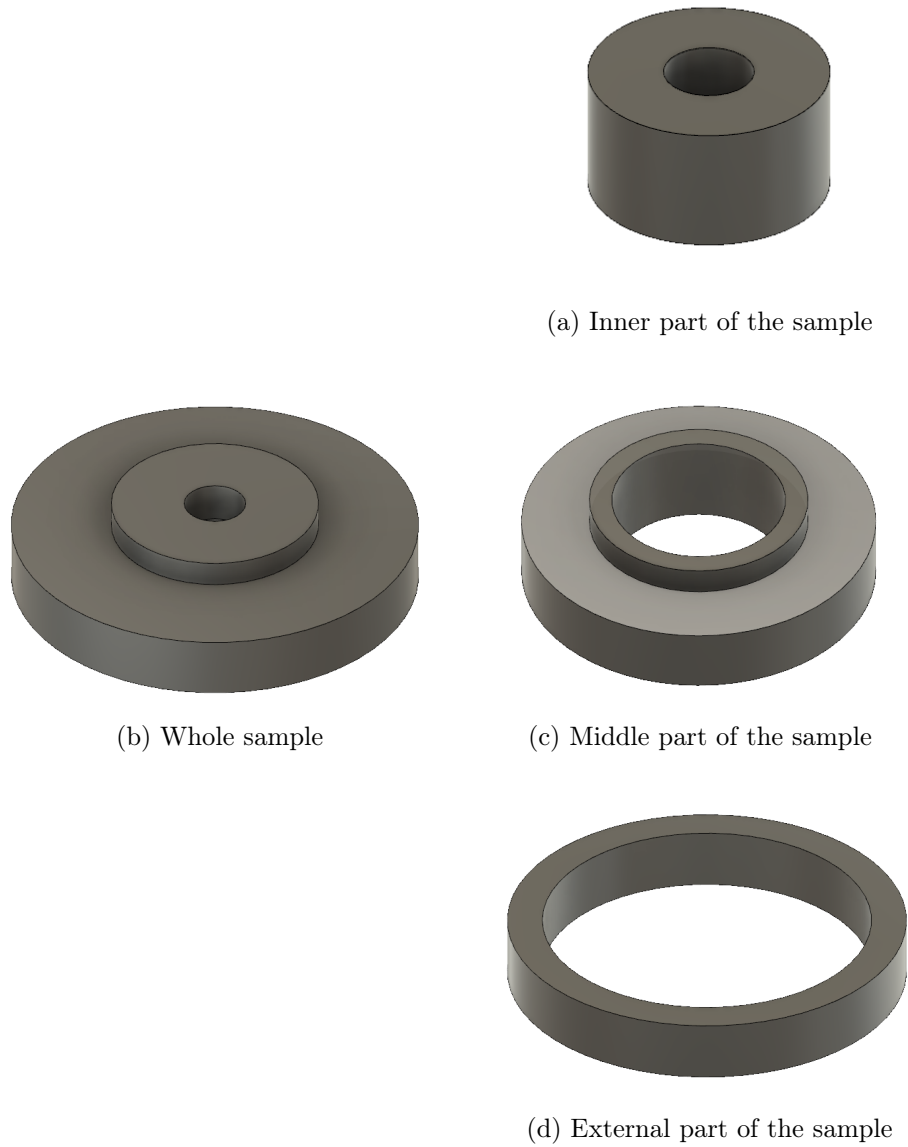(c) Middle part of the sample

(d) External part of the sample

Figure 4.1: Division of the MMC

cold mounting was chosen because an hot mounting could have affected the samples, because of low melting temperature of the aluminium alloy.

4.2.2 Polishing

For the polishing procedure it was used a polisher with changeble sandpaper. The value of sandpaper grit started from a low value of 60, so a rough sandpaper, to
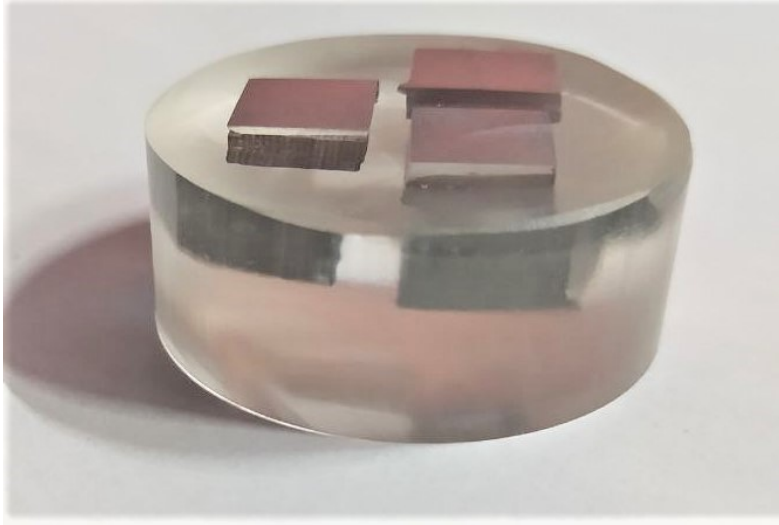
Figure 4.2: Samples incorporated

the high value of 4000 in order to have a smoother surface. After that, it was used a set of special polishers with a diamond suspension at a very low value of grit, 6 µm, 3 µm and 1 µm in order to have a even smoother surface. Also a suspension of colloidal silica was used for the last step of polishing. In the end the surface was smooth but not reflective because of the hardness of silicon carbide which prevented a good polishing.

4.2.3 Chemical attack

A chemical attack was necessary to do to let the precipitates of the aluminium alloy emerge from the material. For the etching of the MMC it was chosen a solution of 1,8 % of fluoboric acid in water, which is an anodizing solution formed by boric acid and fluoridic acid in a solution of $45 - 50\%$.

For this procedure it's necessary a dc current generator, because it's a electrochemical reaction. The procedure for etching the MMC is described as follows: the samples, which are the part to be etched, are connected to the generator as cathode, while the anode is immersed in the solution of fluoboric acid. The sample must be immersed too for the reaction but the cable which connects the sample and the generator must be not in contact with the solution, so it must be well isolated or not immersed. Anode and cathode must be 10 mm apart, and at least 13 mm of anode and cathode must be immersed in solution to permit a correct reaction. The value of current used is 0,16 A/cm² with a voltage of 30 V, and it was mantained for 30 s at 20 °C . After this reaction the sample were immediately placed in water and then dried. Then, the samples were put under a stereo microscope, a special type of microscope which can use polarized light and combinated with a image

processing program can distinguish and colour automatically the grain boundaries in the samples. The pictures were taken on the smoothest areas of the previously polished side. In this experiment the images taken were not coloured because the SiC particles don't permit the correct detection of the grain boundaries, but the images taken are useful for measure the SiC percentage and to look at the precipitates in the grain boundaries to detect the Al alloy. Some example of the final images are in figure 4.3.

4.2.4 Computing of the percentage

A MATLAB code which is in Appendix A were used to compute the percentage of carbides. After this calculation, it can be said that the material is not homogeneous because of the high variance of the SiC powder in the material, as shown in table 4.3. This can be confirmed also from 4.3a, 4.3b, 4.3c.

Sample number	1-1	1-2	1-3	1-4	1-5
Carbide percentage	31,62	33,54	34,76	35,77	31,78
Sample number	2-1	2-2	2-3	2-4	2-5
Carbide percentage	19,24	17,07	31,41	22,22	20,49
Sample number	3-1	3-2	3-3	3-4	3-5
Carbide percentage	36,20	31,65	49,39	36,50	39,57

Table 4.3: Values of percentage of SiC measured.

In the end, it was computed a value of percentage of carbides of:

$$\%_{\text{SiC}} = 31{,}41 \pm 8{,}59\% \tag{4.1}$$

Furthermore, from 4.3a it can be shown the presence of clusters in the material, which will aggravate the tool wear because the tool must cut an hard spot.
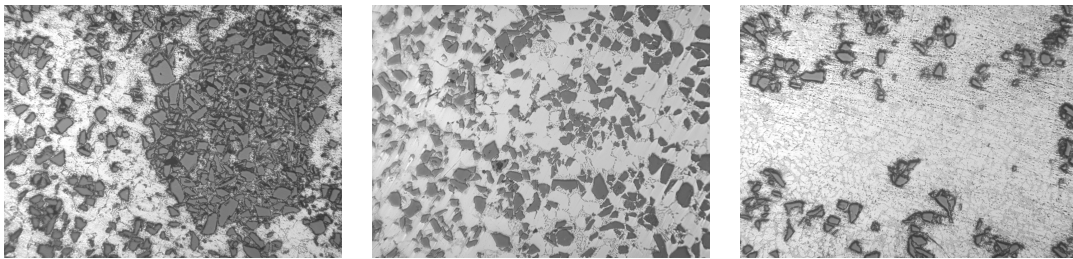
(a) Carbide percentage: 60%   (b) Carbide percentage: 35%   (c) Carbide percentage: 15%

Figure 4.3: Heterogeneousity of the metal matrix composite

4.3   Hardness test

Hardness is a material property which measure the resistance to permanent deformation. It can be quantified with several methods, depending on the hardness of the material, and also differnet tests could not give the same results. For this thesis, a *Rockwell test* was made, which measures the depth of penetration made by an indenter. The indenter can be a diamond cone with a 120° angle, a 1,6 mm or 3,2 mm diameter steel ball. There can be various type of force used for the indentation, which combined with the indenter can give a value named with an acronym, for example HRB or HRC. In table 4.4 there are the cases for the values of characterization of hardness and also the formula to compute the values.

Test	Indenter	Load	Hardness number
A	Diamond cone	60 kg	$HRA = 100 - 500t$
C	Diamond cone	150 kg	$HRC = 100 - 500t$
D	Diamond cone	100 kg	$HRD = 100 - 500t$
B	1,6 mm diameter steel ball	100 kg	$HRB = 130 - 500t$
F	1,6 mm diameter steel ball	60 kg	$HRF = 130 - 500t$
G	1,6 mm diameter steel ball	150 kg	$HRG = 130 - 500t$
E	3,2 mm diameter steel ball	100 kg	$HRE = 130 - 500t$

Table 4.4: Rockwell tests parameters.

It was used previously a diamond indenter but the result of the test was a negative value of hardness, which means the metal matrix compositehardness was too low. So the test was made with the 1,6 mm diameter steel ball in order to have HRB values, in order to have compatible results. The data acquired are shown in table 4.5

Sample number	HRB	HRB	HRB	HRB	HRB	HRB
1	58,0	60,9	60,5	40,2	42,0	54,0
2	47,3	43,8	43,9	46,1	49,6	41,9

Table 4.5: Values of hardness HRB for each test.

From this data, the hardness computed for the metal matrix composite is:

$$HRB = 49,0 \pm 7,5 \tag{4.2}$$

Chapter 5

Setup for the machining experiments

5.1 Machines used for the trials

The turning experiments were carried out on a horizontal *CNC NL 1500 MC 500 Mori Seiki* lathe (5.1a). The *Sensofar Plu Neox^{TM}* optical profiler under focus variation mode was used to quantify the wear (5.1b). The QUANTA scanning electronic microscope SEM was used for the high resolution photos (detector ETD) and also for detection of the tool composition after the machining (detector BSED) (5.1c). The ultrasonic vibration generator Sonomax SX30 was used to permit a controlled oscillation of the tool at a given frequency. It's a particular generator which increase the frequency of electric energy from $50\,\mathrm{Hz}$[1] to a given frequency of $30\,\mathrm{kHz}$. The generator is connected with a coaxial cable to an oscillating system formed by a piezometric transducer and a support for the tool (5.1d).

The setup of the experiments images figure 5.2 and 5.1e emphasize the main oscillating direction which is radial direction, so it can be assumed that this type of oscillation generates an uneven surface as shown in figure 3.7.

5.2 Tool chosen for the trials

A set of 10 PVD TiAlN coated carbide inserts supplied by Sandvik Coromant^{TM} VCGX-11-03-04-AL-1105[2] were used as the cutting tool. The 3D model of the tool and the geometrical dimensions of the tool are explained in 5.3a and 5.3b, and the main properties are exposed in table 5.1.

Cutting parameters recommended from the company are exposed in table 5.2. It was chosen this type of tool because, as explained in section 2.3, there is a lack

---

[1]The supply of italian electric system is set at $50\,\mathrm{Hz}$.

[2]https://www.sandvik.coromant.com/it-it/products/pages/productdetails.aspx?c=VCGX%2011%2003%2004-AL%20%20%20%201105

(a) Lathe used for machining trials.

(b) Profilometer used for wear measurements.

(c) SEM used for trials.

(d) Oscillating system.
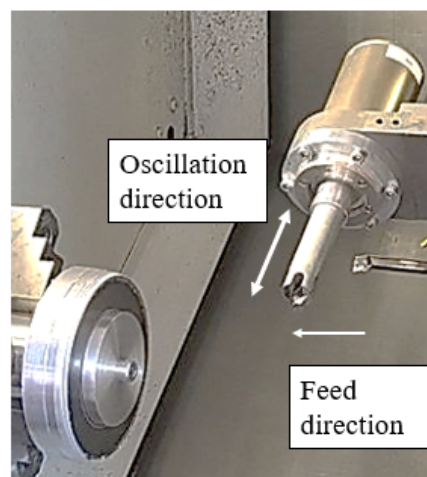
(e) Oscillating direction is the radial direction of the turning operation.

Figure 5.1: Machines used

in literature of studies about cutting metal matrix composites with carbide tools, so an extension of research about those tools is necessary. Moreover, it's necessary to develop the research about this topic to decrease production costs: in fact, the use of PCD and CBN tools is very expensive because of the costs of the tools, but more important is the fact that machining operations on metal matrix composites could cause chipping also on the hardest tools, worsening the characteristics of these tools, for example the sharp edge, and also causing catastrophic failure.
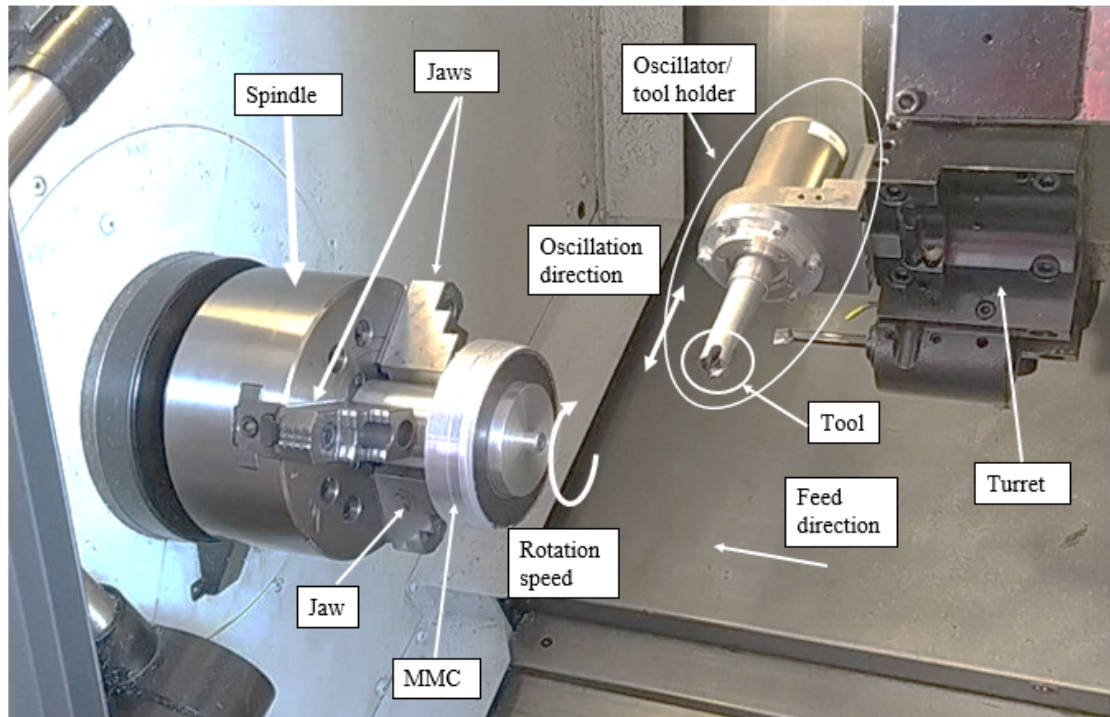
Figure 5.2: Setup of the experiments.

Property	Value
Nose radius	0,397 mm
Length	19,2 mm
Clearance angle	7°
Grade	1105
Material	HC
Type of material	Fine-grained
Coating thickness	Thin
Materials compatible	ISO M: Stainless steels ISO S: Heat Resistant Super Alloys

Table 5.1: Main characteristics of the chosen tool

5.2.1 Cutting parameters selected

From the values recommended from the tool, for previously experiment taken and from literature, they were chosen the parameters exposed in table 5.3.
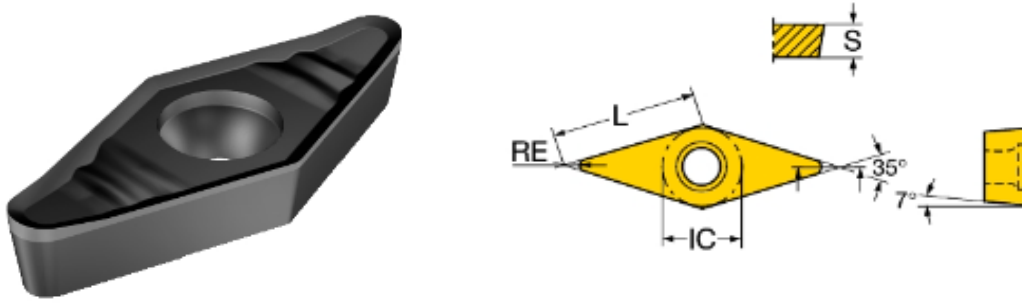
(a) 3D model of the tool selected   (b) Dimensions of the tool selected

Figure 5.3: Tool selected

Cutting parameter	Initial value	Range
Cutting velocity	$75\,\mathrm{m\,min}^{-1}$	
Feed rate	$0{,}06\,\mathrm{mm\,rev}^{-1}$	$0{,}02$ to $0{,}08\,\mathrm{mm\,rev}^{-1}$
Depth of cut	$0{,}5\,\mathrm{mm}$	$0{,}3$ to $1{,}0\,\mathrm{mm}$

Table 5.2: Cutting parameters of the chosen tool

They were chosen four cutting speeds because in the machining theory it's the first parameter that influences tool wear, as shown in section 3.3. Then they were chosen three different feeds because in literature, in particular in [14] it's explained that feed is the main parameter that affects the wear during machining of metal matrix composite, so it's a particular case of general machining theory. After that, two different volume of material were chosen to cut because in literature and also in the ISO regulations [24] it's cited that when there is a strong flank wear mechanism, at the beginning of the cut there is a strong wear rate which then decreases, so two different volumes were necessary to measure the differences of wear rate.

For the ultrasonic vibration assisted turning they were fixed two parameters: the frequency of the vibration $\omega = 30\,\mathrm{kHz}$ and the amplitude of vibration $A = 5\,\mathrm{\mu m}$. From this parameters can be computed the maximum radial speed of the tool, here named *critical speed*:

$$V_{cr} = 2 \cdot \pi \cdot A \cdot \omega = 56{,}5\,\mathrm{m\,min}^{-1} \tag{5.1}$$

5.2.2 Turning trials procedure

First of all, every tool were numbered and associated with a combination of the parameters in table 5.3, in particular with a fixed material removal of $MR = 220\,\mathrm{mm}^3$. After this preliminary part of setting parameters, one by one the machining trials

Cutting parameter	Chosen value
Cutting velocity	20 - 40 - 60 - 120 m/min
Feed rate	0.02 - 0.06 - 0.10 mm/rev
Depth of cut	0.5 mm
Rake angle	0°
Material removed	220 - 660 mm^3

Table 5.3: Cutting parameters of the chosen tool

were done, and also the collecting of chip was done. After every machining trial, every tool was visually worn. Then, a ultrasonic cleaning process with ethanol was necessary in order to have the tool tips as clear as possible for the next step of images acquisition. After this cleaning trial, the photo session was done: in particular, they were taken photos of the tool tip with the SEM in order to visualize the chipping effect using *ETD detector* and also to have a generic composition of the worn tool using *BSED detector*. The profilometers of the flank face were taken with the profilometer in order to measure the flank wear. After the first trial, another cut with a fixed material removal of $MR = 660\,\text{mm}^3$ was done for every tool.

5.2.3   Measurement of wear

First of all, the profilometers of the flank wear with the software sensoSCAN were done. The scanned area was approximately 1.51x1.12 mm with an objective which characteristics are exposed in table 5.4.

Characteristic	Value
Magnification	x20
Field of view	877 x 660 µm
Numerical aperture	0.45
Vertical resolution	8 nm
Lateral resolution	0.31 µm

Table 5.4: Characteristic of the objective used for profilometers

Then, with the software SensoVIEW developed by SensoFAR **SENSOFAR** it was measured the wear. The profilometers were firstly *restored*, in order to have complete set of data points without empty data zones. Then a operation of *form*
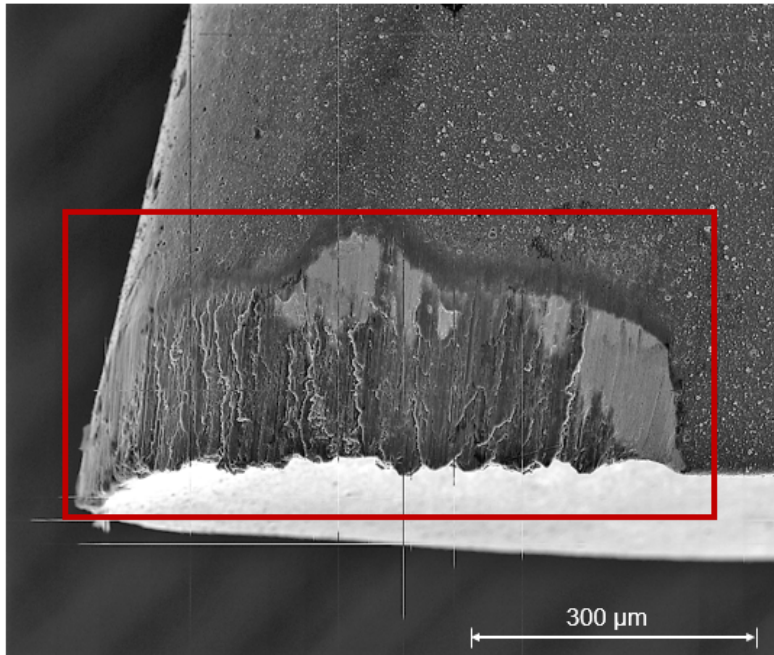
Figure 5.4: SEM images for reference of flank wear

removal was done, in order to set a value of zero to the unworn part of the tool. This operation is shown in, figure 5.5 and figure 5.6 in a 3D view, and in figure 5.7 and figure 5.8 in a 2D view. After that, two lines were draw to visualize the original side of the tool, to measure the real flank wear. Without this operation, the measure will not consider the chipping effect which is the primary wear mechanism in this case. In the end, the measure of maximum flank wear Vb_{max} was done. This procedure was done for all the machining trials.
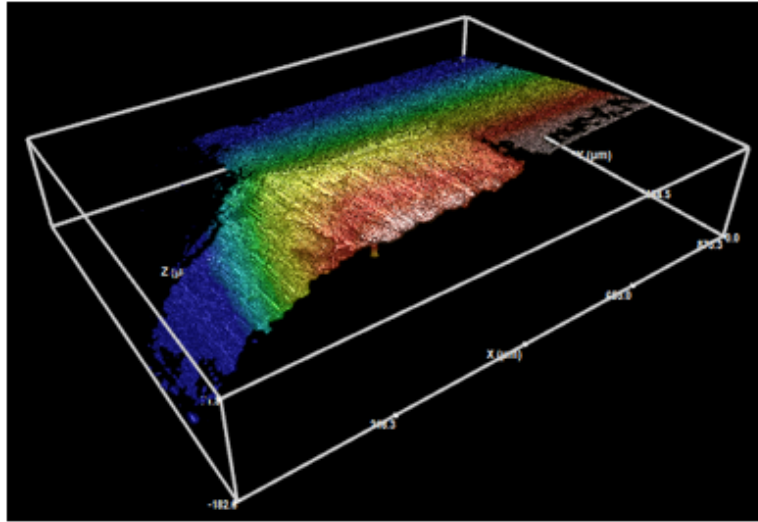
Figure 5.5: 3D profilometer of the tool wear
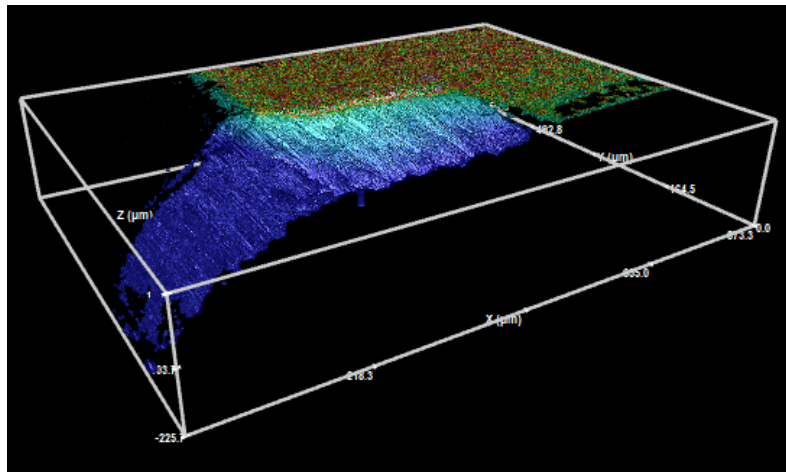
Figure 5.6: 3D profilometer after a flattening correction

5.2.4   Tool etching

In order to measure the tool wear after machining trial with ultrasonic vibration assisted turning, it was necessary to etch the tool tips because of the strong adhesion which prevented a correct measurement. This procedure is destructive so it was done only on the tools which had cut the maximum volume $MR = 660 \, \text{mm}^3$ in order to not affect tools before the complete machining. It was used a *Kroll and Keller* solution made of $3 \, \text{mL}$ of hydrofluoric acid HF and $6 \, \text{mL}$ of nitric acid HNO_3 in $100 \, \text{mL}$ of water. Then the tools were immersed in the solution for 10 minutes and then cleaned in water. After that, the tools were ready for the measurement
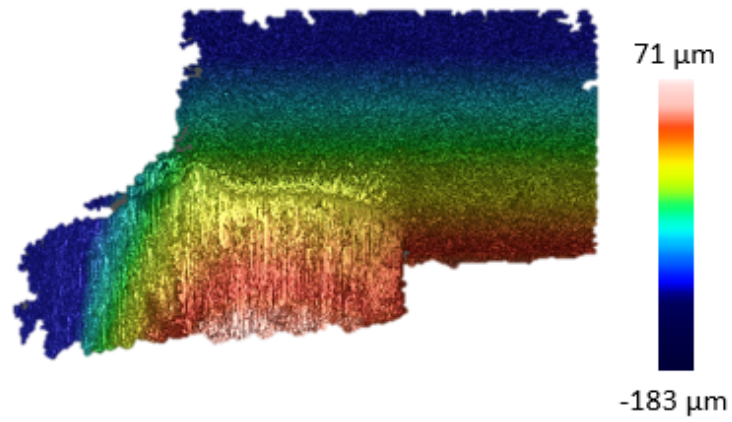
Figure 5.7: 2D profilometer of the tool wear
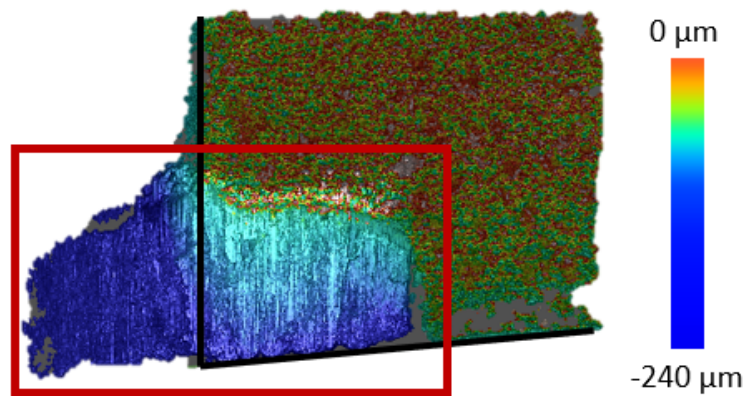
Figure 5.8: 2D profilometer after a flattening correction. The black lines are the reference in respect of the unworn tool.

explained in subsection 5.2.3. An example of etching trial is shown in figure 5.10. After the etching it was made also an *Energy Dispersive X-ray Spectroscopy EDS* to understand the composition of the material on the tool after the machining. Every image reported below has in the right the EDS spectrum for every different material, so it can be said that for every image the light grey part is the TiAlN coating of the tool, the white part is the WC under the coating, which is the main component of the tool, and the dark grey part is adhesion of the MMC on the tip.
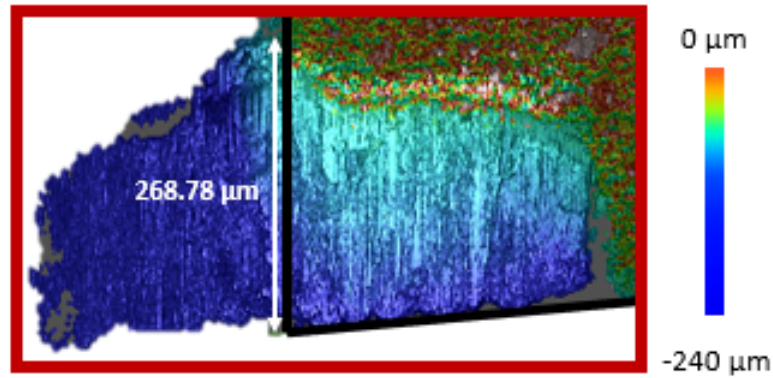
Figure 5.9: Zoom of the figure 5.8 on the wear part. The measure of wear can be done directly with the tools of sensoVIEW.
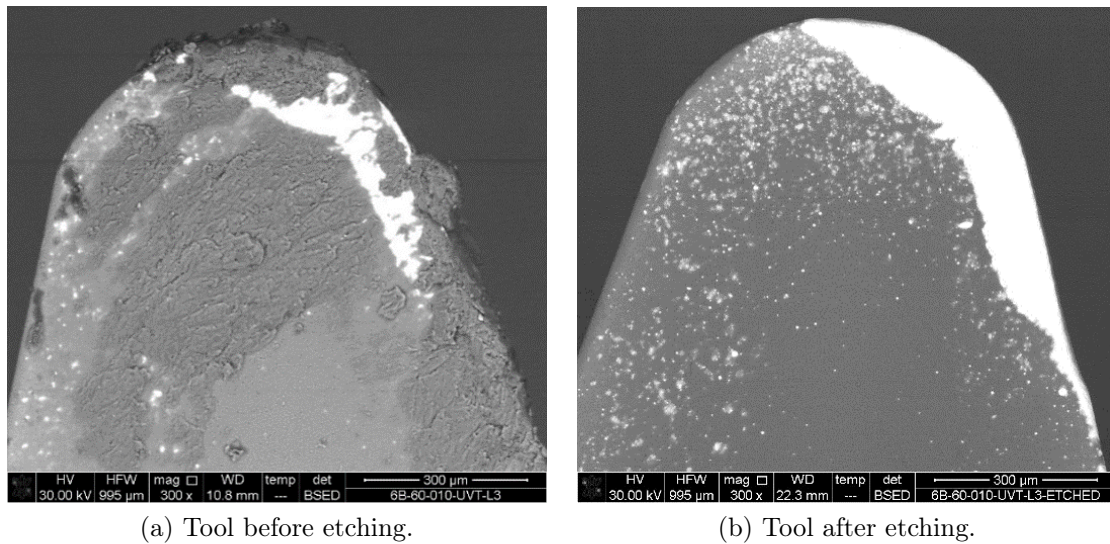
(a) Tool before etching.

(b) Tool after etching.

Figure 5.10: Adhesion on a tool at feed of $f = 0{,}10\,\mathrm{mm\,rev^{-1}}$, cutting speed of $V_c = 60\,\mathrm{m\,min^{-1}}$ and material removal of $MR = 660\,\mathrm{mm^3}$ using ultrasonic vibration assisted turning
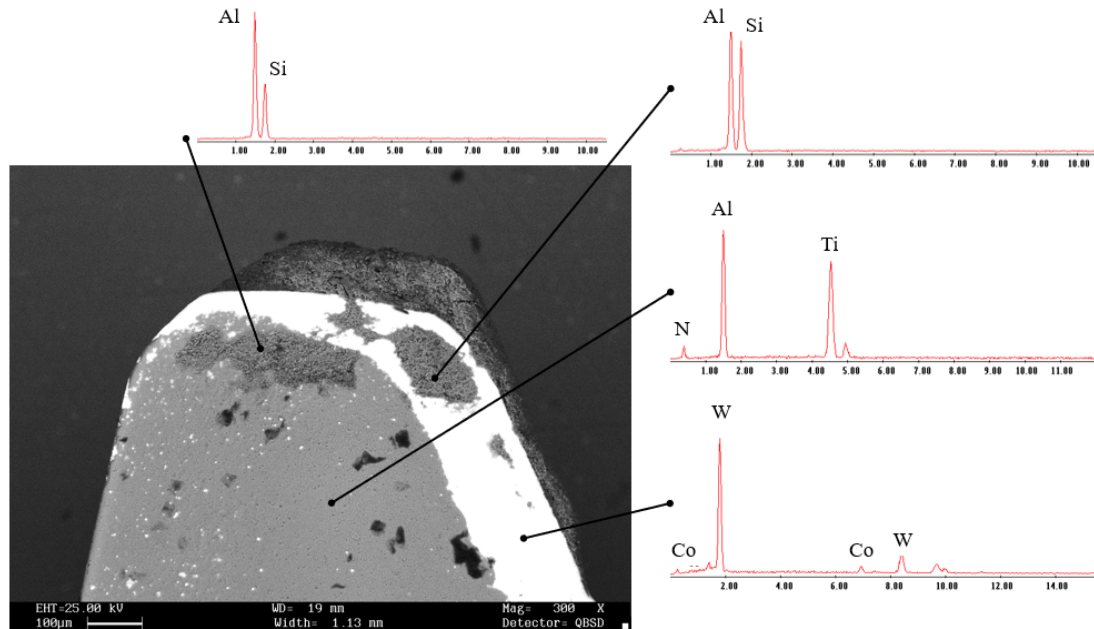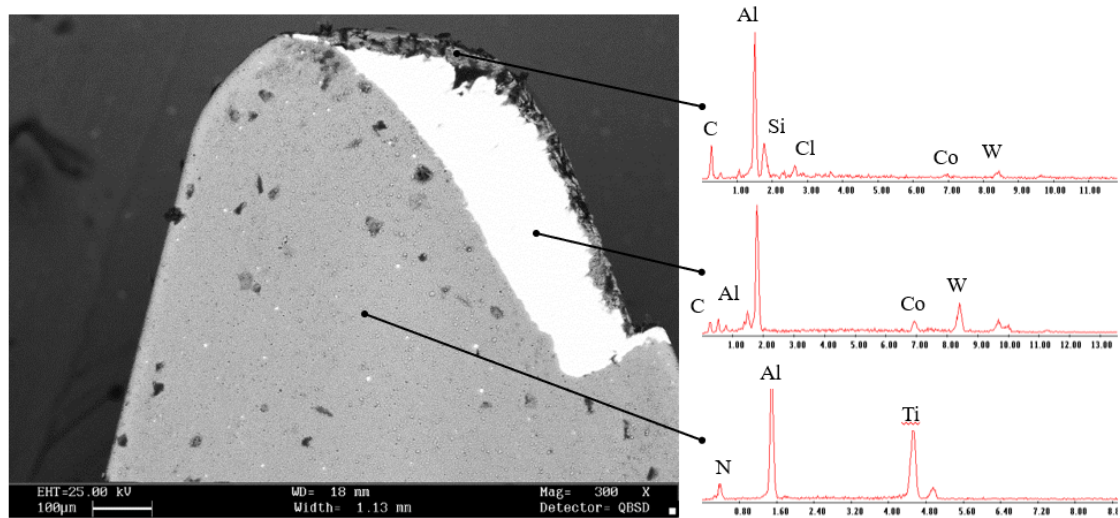
37
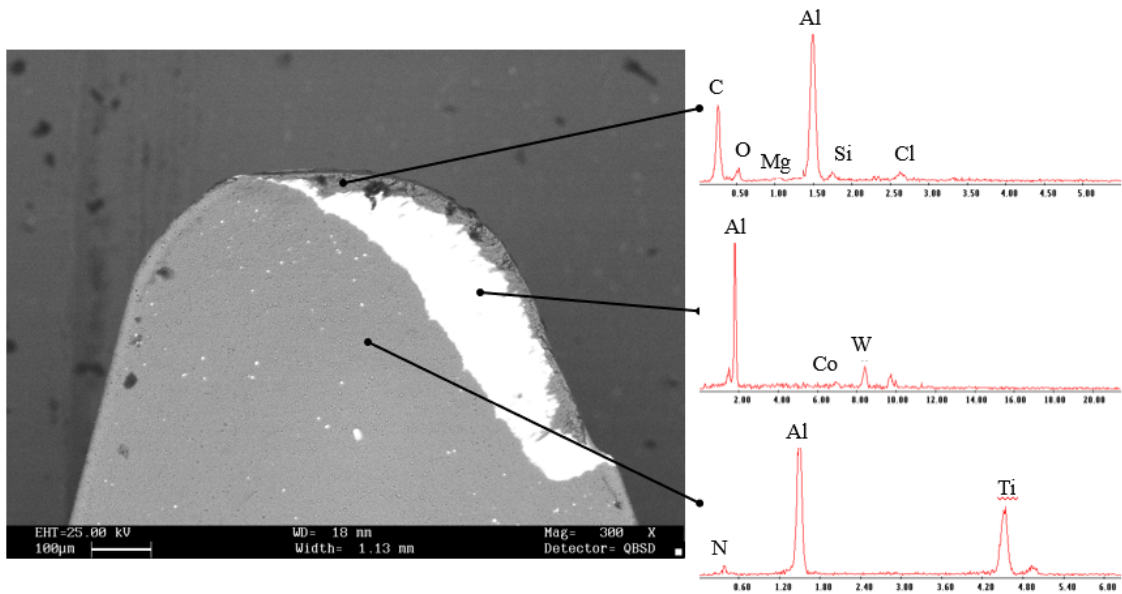
Figure 5.11: Tool before etching: feed of $f = 0{,}06\,\mathrm{mm\,rev^{-1}}$, cutting speed of $V_c = 60\,\mathrm{m\,min^{-1}}$ and material removal of $MR = 660\,\mathrm{mm^3}$ using conventional turning
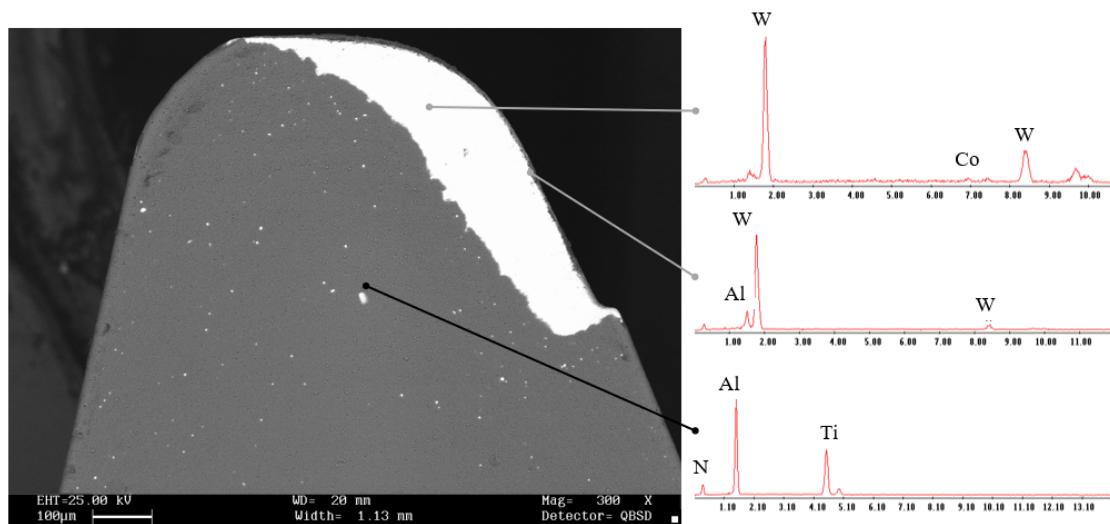
Figure 5.12: Tool after etching: feed of $f = 0{,}06\,\mathrm{mm\,rev^{-1}}$, cutting speed of $V_c = 60\,\mathrm{m\,min^{-1}}$ and material removal of $MR = 660\,\mathrm{mm^3}$ using conventional turning

38
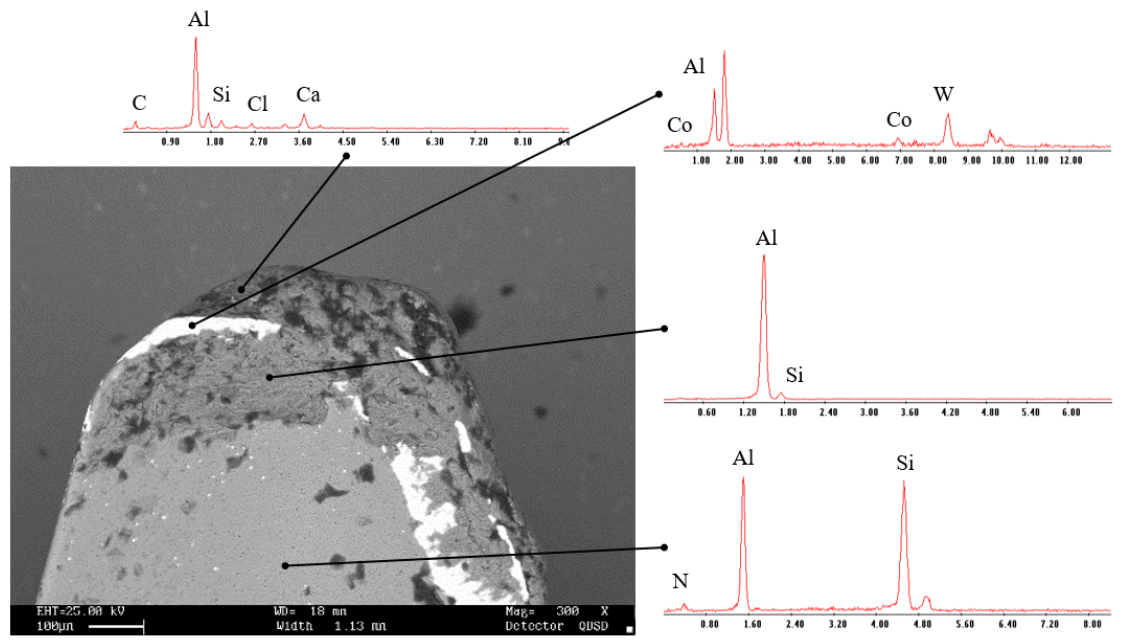
Figure 5.13: Tool before etching: feed of $f = 0{,}06\,\mathrm{mm\,rev^{-1}}$, cutting speed of $V_c = 60\,\mathrm{m\,min^{-1}}$ and material removal of $MR = 660\,\mathrm{mm^3}$ using ultrasonic vibration assisted turning
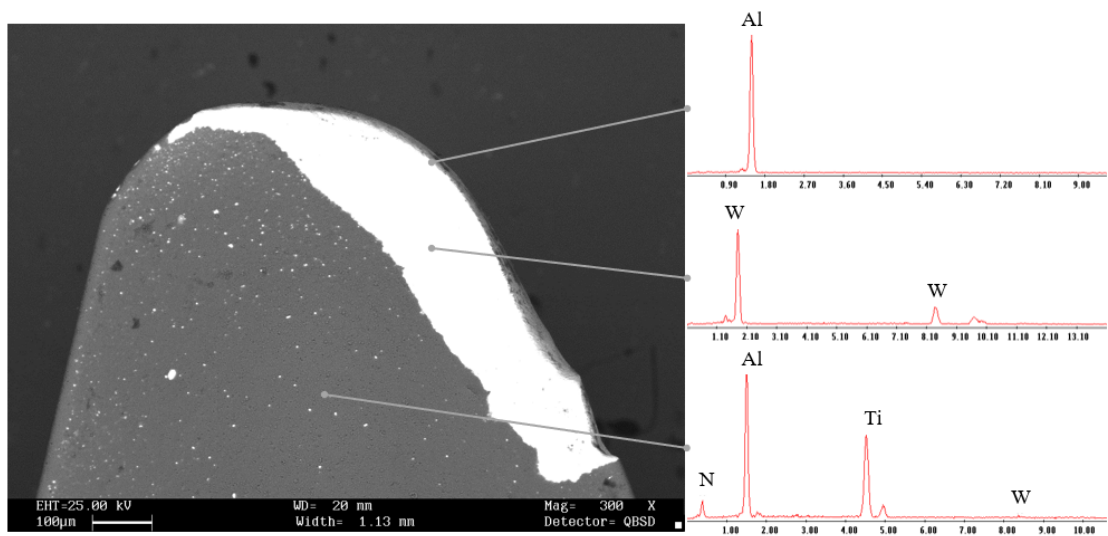

Figure 5.14: Tool after etching: feed of $f = 0{,}06\,\mathrm{mm\,rev^{-1}}$, cutting speed of $V_c = 60\,\mathrm{m\,min^{-1}}$ and material removal of $MR = 660\,\mathrm{mm^3}$ using ultrasonic vibration assisted turning

39

Figure 5.15: Tool before etching: feed of $f = 0{,}06\,\mathrm{mm\,rev^{-1}}$, cutting speed of $V_c = 120\,\mathrm{m\,min^{-1}}$ and material removal of $MR = 660\,\mathrm{mm^3}$ using conventional turning
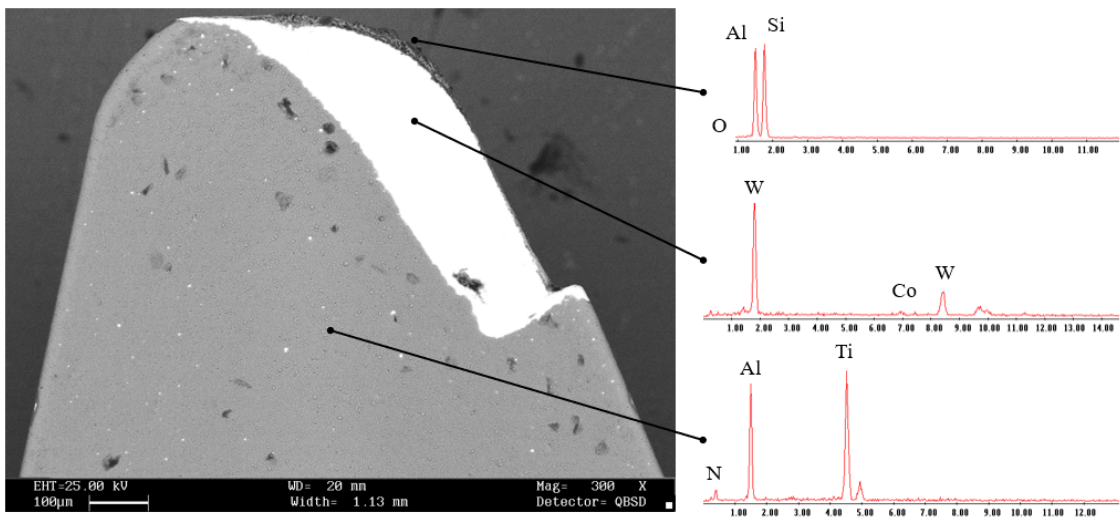
Figure 5.16: Tool after etching: feed of $f = 0{,}06\,\mathrm{mm\,rev^{-1}}$, cutting speed of $V_c = 120\,\mathrm{m\,min^{-1}}$ and material removal of $MR = 660\,\mathrm{mm^3}$ using conventional turning
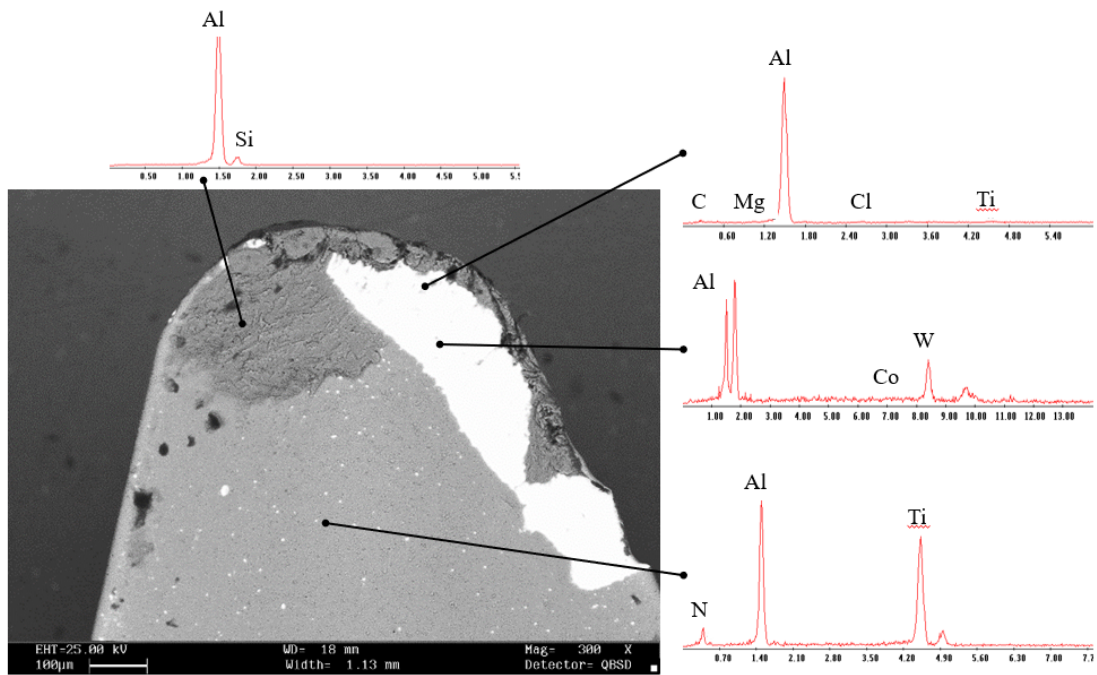
Figure 5.17: Tool before etching: feed of $f = 0{,}06\,\mathrm{mm\,rev^{-1}}$, cutting speed of $V_c = 120\,\mathrm{m\,min^{-1}}$ and material removal of $MR = 660\,\mathrm{mm^3}$ using ultrasonic vibration assisted turning

Figure 5.18: Tool after etching: feed of $f = 0{,}06\,\mathrm{mm\,rev^{-1}}$, cutting speed of $V_c = 120\,\mathrm{m\,min^{-1}}$ and material removal of $MR = 660\,\mathrm{mm^3}$ using ultrasonic vibration assisted turning

41

Chapter 6

Results

In this chapter are exposed the data obtained of the tool wear with the method and cutting conditions described in chapter 5. The results of wear are then shown in function of the main cutting parameters, so the effect of conventional turning versus ultrasonic vibration assisted turning, the effect of cutting speed, feed and also of different volume of material removal. Then the data will be compared with the classic machining theory to see if the tool life can be represented with Taylor's wear law. After that, there will be analysed the chips obtained in the machining process, in particular the chip type.

6.1 Type of wear

Type of wear found in this research is a combination of *chipping*, *adhesion* and *abrasion* wear. In particular, adhesion of workpiece material on tool, *built-up edge* (BUE), cause chipping. This happens because BUE is mechanically unstable [11] so after its formation, the cutting forces on the tool detach the BUE, removing also part of the tool because of adhesion between tool material and the workpiece. In all the trials the first part removed from the tool is the cutting edge, and after that the SiC particles of the workpiece further abrade the tool around the cutting edge: in particular, the flank wear is given by the abrasion of the particles of the finished part, and the rake wear is given by the abrasion of SiC particles in the chips.

6.2 Effect of cutting speed

Cutting speed is the first parameter analysed because according to classic theory of machining, it's the main parameter which influences mainly the tool wear, as explained in section 3.3, so it's oblivious to prioritize the results of this parameter.

In 6.1a, 6.3a, 6.5a, 6.2a, 6.4a and 6.6a are shown the values of flank wear in function of cutting speed, with a fixed feed and a fixed volume of material removed

in both cases of conventional turning and ultrasonic vibration assisted turning.

6.2.1 $f = 0{,}02\,\mathrm{mm\,rev^{-1}}$

In 6.1a it's shown that during conventional turning the wear increases with speed, as confirmed by the classic machining theory. Another behaviour is found with ultrasonic vibration assisted turning: flank wear decreases slightly, so there is a maximum of wear at $V_c = 60\,\mathrm{m\,min^{-1}}$. In 6.2a it's shown that in both cases of conventional turning and ultrasonic vibration assisted turning the wear increases with speed, as confirmed by the theory, so it can be said that increasing the volume of material removal the flank wear has a predictable behaviour. Also, another detail can be enlighted: the adhesion affects the measurement of wear and it couldn't be removed at $MR = 220\,\mathrm{mm^3}$ because the same tool was used also for the measurement of wear at $MR = 660\,\mathrm{mm^3}$.

Excluding the last data, it can be said that at low feed $f = 0{,}02\,\mathrm{mm\,rev^{-1}}$ the flank wear follows the classic wear theory of machining.

6.2.2 $f = 0{,}06\,\mathrm{mm\,rev^{-1}}$

In 6.3a it's shown that during conventional turning the flank wear has a counter-intuitive behaviour: in fact, there is a decreasing of flank wear from $V_c = 20\,\mathrm{m\,min^{-1}}$ to $V_c = 40\,\mathrm{m\,min^{-1}}$, then the flank wear increases with cutting speed, so there is a minimum of flank wear at $V_c = 40\,\mathrm{m\,min^{-1}}$. During ultrasonic vibration assisted turning the flank wear increases with cutting speed, according with the classic theory. In 6.4a it's shown that during conventional turning the flank wear increases with cutting speed, according with the classic theory. During ultrasonic vibration assisted turning the flank wear has a counter-intuitive behaviour: in fact, there is an intense increasing of flank wear from $V_c = 40\,\mathrm{m\,min^{-1}}$ to $V_c = 60\,\mathrm{m\,min^{-1}}$, then the flank wear decreases with cutting speed, so there is a maximum of flank wear at $V_c = 60\,\mathrm{m\,min^{-1}}$. This is due to the strong adhesion which affected the tool and prevented a correct measurement, as shown in 6.4h. Excluding the last data, it can be said that at low feed $f = 0{,}06\,\mathrm{mm\,rev^{-1}}$ the flank wear follows the classic wear theory of machining.

6.2.3 $f = 0{,}10\,\mathrm{mm\,rev^{-1}}$

In 6.5a it's shown that the wear remains almost constant with cutting speed and also there is no difference between conventional turning and ultrasonic vibration assisted turning. In 6.6a it's shown that the wear remains almost constant with cutting speed during conventional turning but using ultrasonic vibration assisted turning the wear increases with cutting speed.

It can be seen that generally the flank wear increases with cutting speed both with conventional turning and ultrasonic vibration assisted turning, so the behaviour is the same expected with the classic theory of machining where the wear can be modeled with Taylor's equation Equation 3.10.

It can be also noticed that there are some particular conditions, when the cutting speed at $V_c = 60\,\mathrm{m\,min^{-1}}$ in which there is the maximum adhesion obtained in this trials.

This behaviour happens with every feed tested so it can be said that in general *to limit tool wear must be used a* **low cutting speed**.

6.3   Effect of feed rate

This is the second parameter analysed because during machining of monolithic alloys it's common to find that high feed causes high forces and so higher tool wear, but during machining of metal matrix composite the abrasion wear due to the hard reinforcements is higher than the increase of the forces due to high feed, so it's better to have an high feed to have less machining time and so less abrasion wear [14].

In 6.7a, 6.9a, 6.8a, 6.10a are shown the values of flank wear in function of feed, with a fixed cutting speed and a fixed volume of material removed in both cases of conventional turning and ultrasonic vibration assisted turning.

6.3.1 $V_c = 60\,\mathrm{m\,min^{-1}}$

In 6.7a it's shown that flank wear decreases with feed in both cases of conventional turning and ultrasonic vibration assisted turning. In particular for the conventional turning from $f = 0{,}06\,\mathrm{mm\,rev^{-1}}$ to $f = 0{,}10\,\mathrm{mm\,rev^{-1}}$ the flank wear stabilises at the same value. Another detail that can be noticed is that the flank wear is greater during ultrasonic vibration assisted turning than during conventional turning. This is caused by the adhesion which affected the measurements. In 6.9a it's shown that flank wear decreases with feed during conventional turning, in particular from $f = 0{,}06\,\mathrm{mm\,rev^{-1}}$ to $f = 0{,}10\,\mathrm{mm\,rev^{-1}}$ the flank wear stabilises at the same value. During ultrasonic vibration assisted turning there is a peak of flank wear at $f = 0{,}06\,\mathrm{mm\,rev^{-1}}$ which is probably due to adhesion effect. The other values of flank wear are smaller than the values during conventional turning.

Excluding the last data, it can be said that at low speed $V_c = 60\,\mathrm{m\,min^{-1}}$ the flank wear decreases with feed, so if it's necessary to machine an high volume of material it's better using ultrasonic vibration assisted turning.

6.3.2 $V_c = 120\,\mathrm{m\,min^{-1}}$

In 6.8a it's shown that flank wear decreases with feed in both cases of conventional turning and ultrasonic vibration assisted turning. In particular for the ultrasonic vibration assisted turning from $f = 0{,}02\,\mathrm{mm\,rev^{-1}}$ to $f = 0{,}06\,\mathrm{mm\,rev^{-1}}$ the flank wear stabilises at the same value. Another detail that can be noticed is that the flank wear is greater during ultrasonic vibration assisted turning than during conventional turning. This is caused by the adhesion which affected the measurements. In 6.10a it's shown that flank wear decreases with feed during both conventional turning and ultrasonic vibration assisted turning, and the flank wear is smaller during ultrasonic vibration assisted turning.

So, it can be said that at high speed $V_c = 120\,\mathrm{m\,min^{-1}}$ flank wear decreases with feed, so in the end it can be said that the results found are the same of [14], and they are counter-intuitive because they are opposite to the classic theory of machining: in each case, ***the increasing of feed cause a decreasing of flank wear***.

This peculiar behaviour can be explained as follows: assuming a fixed material removal, if feed is low, the cutting distance of the tool will be high, so the abrasion effect of reinforcements will be maintained for a longer time, giving in the end a bigger flank wear. This phenomena is shown in 6.11a, 6.11c and 6.11e, where the black lines are the hypothetical feed marks made from the cutting edge. In 6.11b, 6.11d and 6.11f there is also the rapresentation of the distance traveled by the tool in a 3D viev for every feed.

6.4 Effect of ultrasonic vibration assisted turning

The effect of assisted turning was briefly discussed before, here summarised:

in 6.1a it's shown that using ultrasonic vibration assisted turning the flank wear is lower than using conventional turning, and in particular the wear decreases with increasing speed. In 6.2a, so with an increase of material removed, ultrasonic vibration assisted turning has a lower tool wear, difference between ultrasonic vibration assisted turning and conventional turning decreases, and there is an increase of wear with the cutting speed, as seen in classic theory.

In 6.3a it's shown that using ultrasonic vibration assisted turning the flank wear is lower using conventional turning than ultrasonic vibration assisted turning, except when the cutting speed is very low, so at $V_c = 20\,\mathrm{m\,min^{-1}}$. In 6.4a, so with an increase of material removed, ultrasonic vibration assisted turning has a lower tool wear except when $V_c = 60\,\mathrm{m\,min^{-1}}$.

In 6.5a it's shown that the wear of tools doesn't change from ultrasonic vibration assisted turning and conventional turning. In 6.6a, so with an increase of material removed, ultrasonic vibration assisted turning has a lower tool wear. It's noteworthy that at cutting speed of $V_c = 60\,\mathrm{m\,min^{-1}}$ the wear increases slightly with material

removed. So, in the end it can be said that for certain values of Cutting speed and feed, ***ultrasonic vibration assisted turning decreases tool wear***.

6.4.1   Adhesion on tools

Using ultrasonic vibration assisted turning has an important effect which affects directly the wear of tools: in fact, the vibrational motion given to the tool increase the total speed of the tool, so the real tool speed is greater than the cutting speed, as shown in Equation 6.1 and in figure 6.12:

$$V_{tool_{max}} = \sqrt{V_c^2 + V_c r^2} \geq V_c \tag{6.1}$$

This will lead to an increase of friction on the tool so the temperature increases as well, causing the formation of adhesion of the workpiece on the tool tip, causing the BUE.

In general adhesion depends on cutting speed, feed, and happens also using conventional turning. In almost all machining trials there were adhesion on tool but there were some particular cases in which the adhesion was so abundant that prevented the correct measurement of wear, as exposed in subsection 5.2.4. These particular cases are: material removal of $MR = 660\,\mathrm{mm}^3$, feed of $f = 0{,}06\,\mathrm{mm\,rev}^{-1}$ and $f = 0{,}10\,\mathrm{mm\,rev}^{-1}$, cutting speed of $V_c = 60\,\mathrm{m\,min}^{-1}$ during ultrasonic vibration assisted turning.

An interpretation of this behaviour is that there is a balancing effect between cutting speed and temperature in the tool: in fact, at high cutting speed the BUE is smaller because of forces that break it, but at low cutting speed the breaking of the BUE is counterbalanced by the gain of adhesion given by the increase of temperature caused by ultrasonic vibration assisted turning, leading to the maximum adhesion possible at $V_c = 60\,\mathrm{m\,min}^{-1}$. There is also the feed effect that can be discuss: in fact, at low feed there is less adhesion because of the high abrasion wear caused by reinforcement in the workpiece, while at high feed the adhesion is much more. An effect of the material removed can be discuss as well: in fact, the increase of material machined lead to an increase of wear in the rake face and in the flank as well, causing an irregular surface on the tool tip which cause an increase of friction and temperature.

6.5   Chip formation

During machinng trials were collected also the chips, and were found four different types of chip shapes. All of these chip shapes have a common characteristic: during formation, the chips deforms in a way to form a spiral around a straight axis, known as the main axis of the chip. The cause of spinning during generation axis is shown in 6.13a: friction between chip and tool on the rake face generates heat, which

cause a local increase of temperature leading to an additional deformation, so total deformation in the tool side is greater than the deformation on the free side, causing the rotation of the chip.

For every chip it's defined: width of the chip w, thickness of the chip t_c, the chip surface, the normal to the surface, and the chip axis, as shown in figure 6.14. Every chip type has differences regarding the dimensions.

The type of chips found are four: *Conical type*, *Washer-type*, *C-shape*, and *Tubular*.

6.5.1 Tubular

Tubular is the most simple of all the chips found and also the most common found in this work: the chips remain parallel to the initial chip orientation, and so perpendicular to the finished surface, because the tool gives a constant deformation along the chip width, as shown in figure 6.15. It generates only in condition of no adhesion on the tool, or in the particular case when adhesion compensate the tool wear, so from the point of view of the chip, the tool is still intact and so tubular chip forms.

6.5.2 Conical

Conical chips: width direction of the chip is inclined by an angle β between 0° and 90° in respect to the chip axis, as shown in figure 6.16. Conical chips generate because of the BUE on the tool which works as an enlargement of the tool tip, causing a non-homogeneous deformation along the chip width.

6.5.3 Washer-type helical chips

Washer-type helical chips generate in the same way of the conical-type chips, but the main difference is that adhesion is greater, so the resulting chip is rotated of almost 90°.

6.5.4 C-shape

C – shape was found at the lowest feed f = 0.02 mm/rev and during UVT. It happens in this condition because at low feed the chip has a low thickness, so the chip will break easily if submitted by a strain.

6.6 Final valuation of results

This combination of material and tool at the end takes place as a particular case on the big subject of machining process. Infact, it determines that the use of ultrasonic

vibration assisted turning decrease the tool wear, which is counter-intuitive because vibrations on machining are always avoided as much as possible, because of the variation of forces that cause an high tool wear and a worsening of surface roughness. Also, it took place another counter-intuitive results about feed: tool wear decrease with the increase of feed. This is caused by the fact that high feed, with fixed cutting speed and length of the workpiece, the *spiral cutting length* decreases, so the distance traveled by the tool is lower and so the contact time between cutting edge and reinforcements is lower, causing a lowering of wear.

The resume of all these results is that setting an high feed ($f = 0{,}10\,\mathrm{mm\,rev^{-1}}$), a low cutting speed ($V_c = 60\,\mathrm{m\,min^{-1}}$) using ultrasonic vibration assisted turning method it's the best condition to machine the MMC in a roughing process, because of the low initial chipping and the low flank wear after an high volume of machined material.
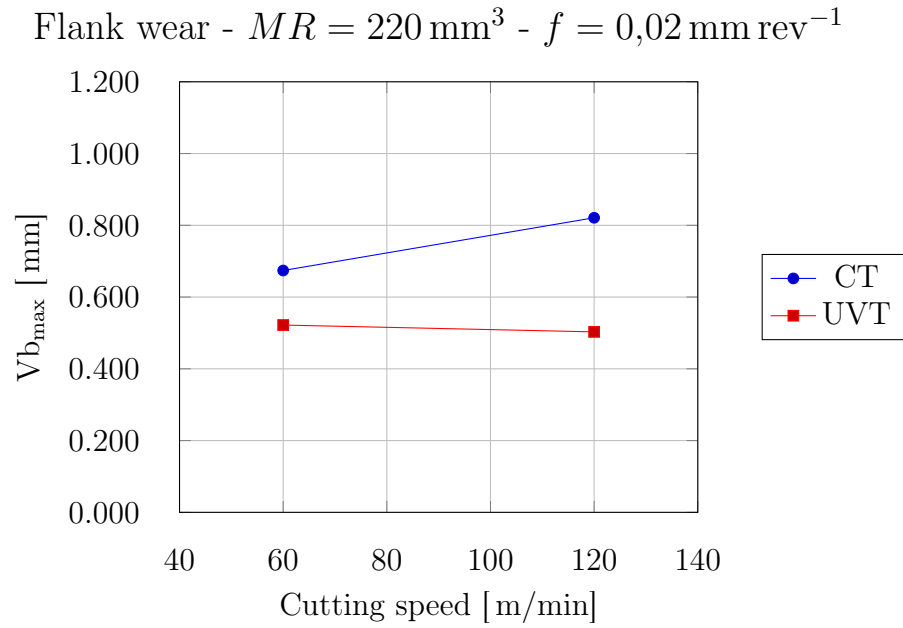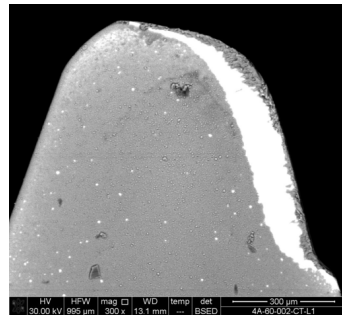
Flank wear - $MR = 220\,\text{mm}^3$ - $f = 0{,}02\,\text{mm}\,\text{rev}^{-1}$

(a) flank wear in function of cutting speed

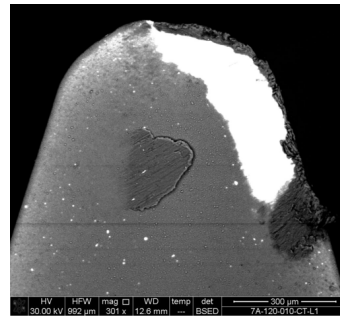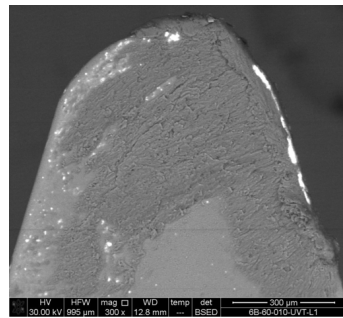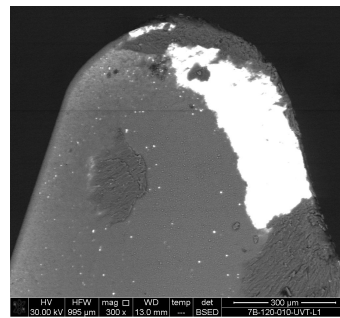(b) conventional turning
$V_c = 60\,\text{m}\,\text{min}^{-1}$
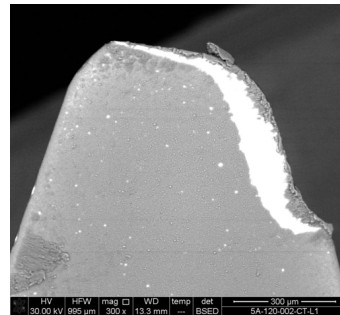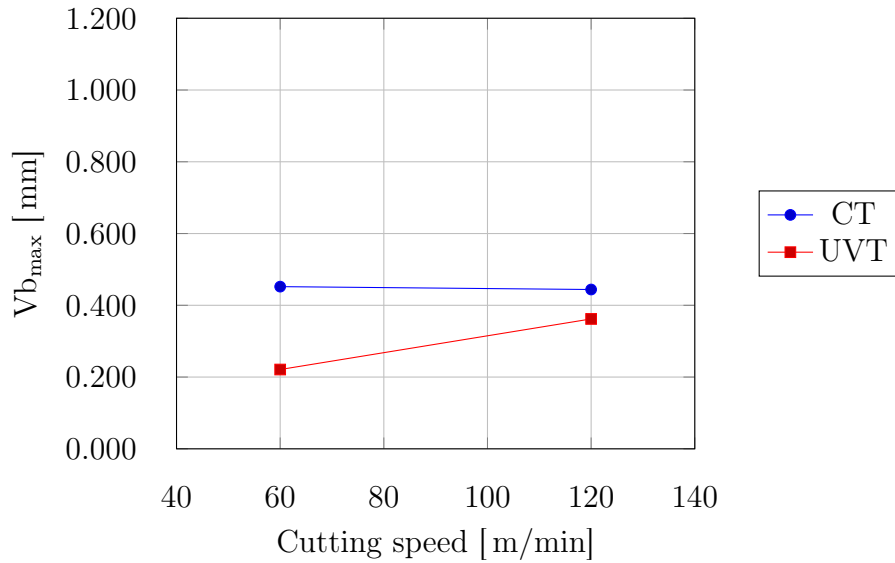

(c) conventional turning
$V_c = 120\,\text{m}\,\text{min}^{-1}$
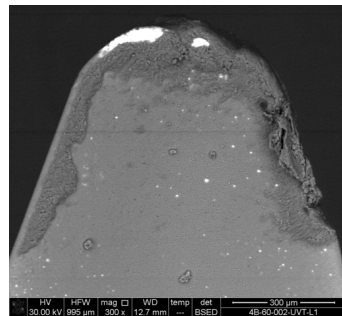
(d) ultrasonic vibration
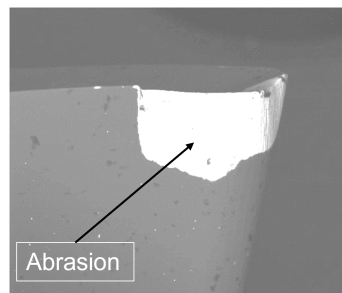assisted turning
$V_c = 60\,\text{m}\,\text{min}^{-1}$
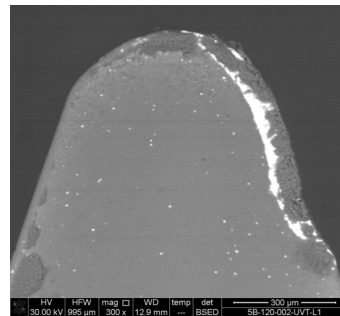
(e) ultrasonic vibration
assisted turning
$V_c = 120\,\text{m}\,\text{min}^{-1}$

Figure 6.1: Effect of cutting speed at a fixed material removal of $MR = 220\,\text{mm}^3$ and feed of $f = 0{,}02\,\text{mm}\,\text{rev}^{-1}$
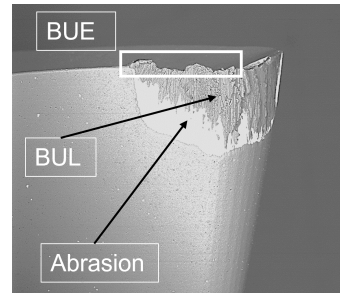
Flank wear - $MR = 660\,\mathrm{mm}^3$ - $f = 0{,}02\,\mathrm{mm\,rev}^{-1}$
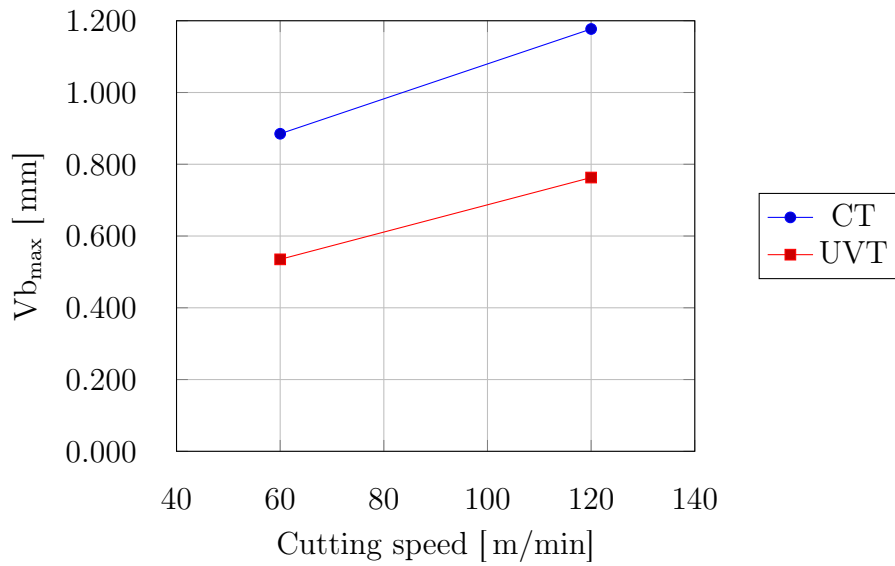
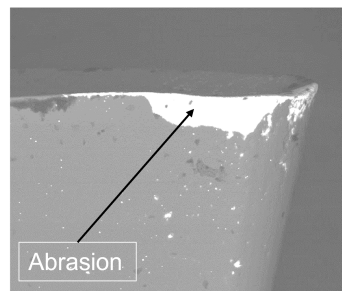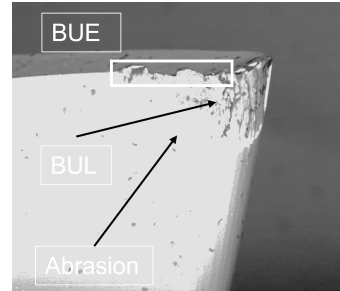(a) flank wear in function of cutting speed
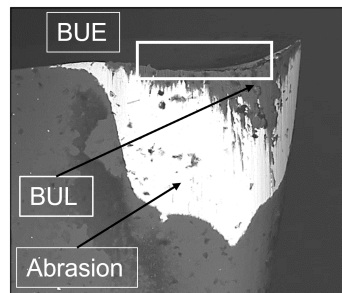
(b) conventional turning
$V_c = 60\,\mathrm{m\,min}^{-1}$
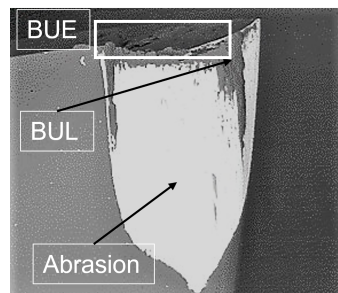
(c) conventional turning
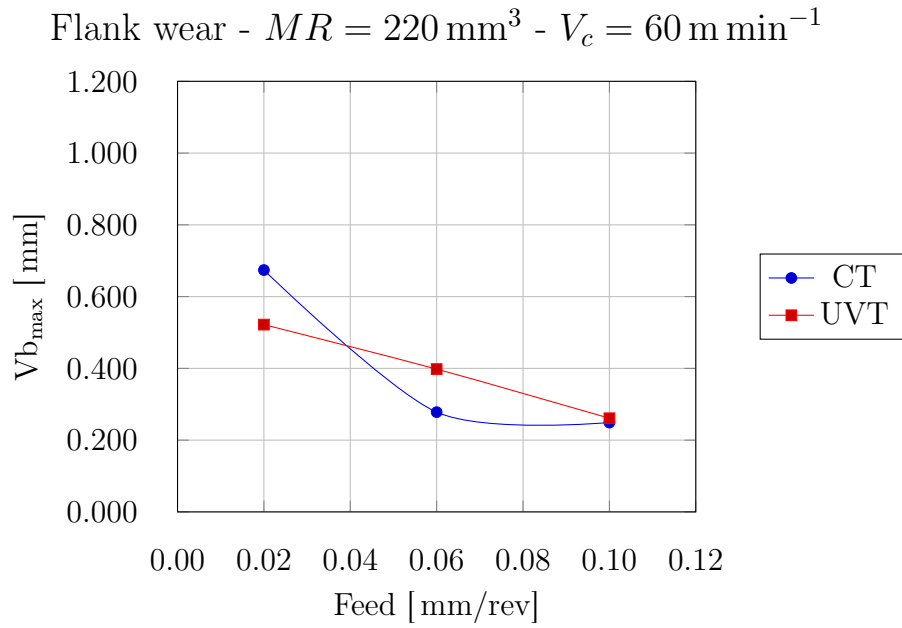$V_c = 120\,\mathrm{m\,min}^{-1}$
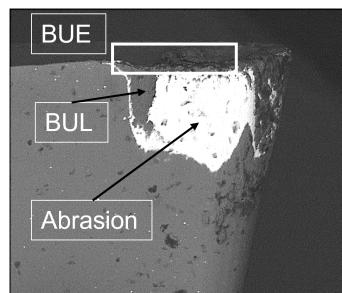
(d) ultrasonic vibration
assisted turning
$V_c = 60\,\mathrm{m\,min}^{-1}$
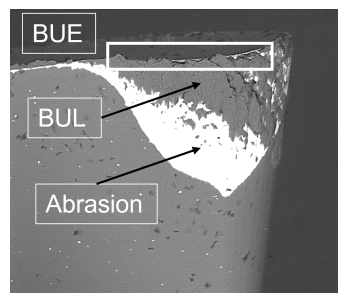
(e) ultrasonic vibration
assisted turning
$V_c = 120\,\mathrm{m\,min}^{-1}$

Figure 6.2: Effect of cutting speed at a fixed material removal of $MR = 660\,\mathrm{mm}^3$ and feed of $f = 0{,}02\,\mathrm{mm\,rev}^{-1}$

Flank wear - $MR = 220\,\mathrm{mm}^3$ - $f = 0{,}06\,\mathrm{mm\,rev}^{-1}$

(a) flank wear in function of cutting speed

(b) conventional turning $V_c = 20\,\mathrm{m\,min}^{-1}$

(c) conventional turning $V_c = 40\,\mathrm{m\,min}^{-1}$

(d) conventional turning $V_c = 60\,\mathrm{m\,min}^{-1}$

(e) conventional turning $V_c = 120\,\mathrm{m\,min}^{-1}$

(f) ultrasonic vibration assisted turning $V_c = 20\,\mathrm{m\,min}^{-1}$

(g) ultrasonic vibration assisted turning $V_c = 40\,\mathrm{m\,min}^{-1}$

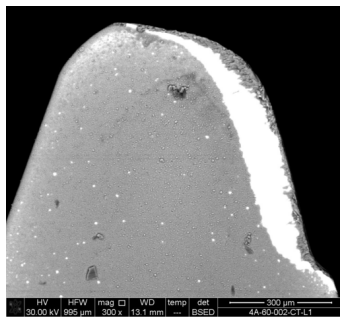(h) ultrasonic vibration assisted turning $V_c = 60\,\mathrm{m\,min}^{-1}$

(i) ultrasonic vibration assisted turning $V_c = 120\,\mathrm{m\,min}^{-1}$
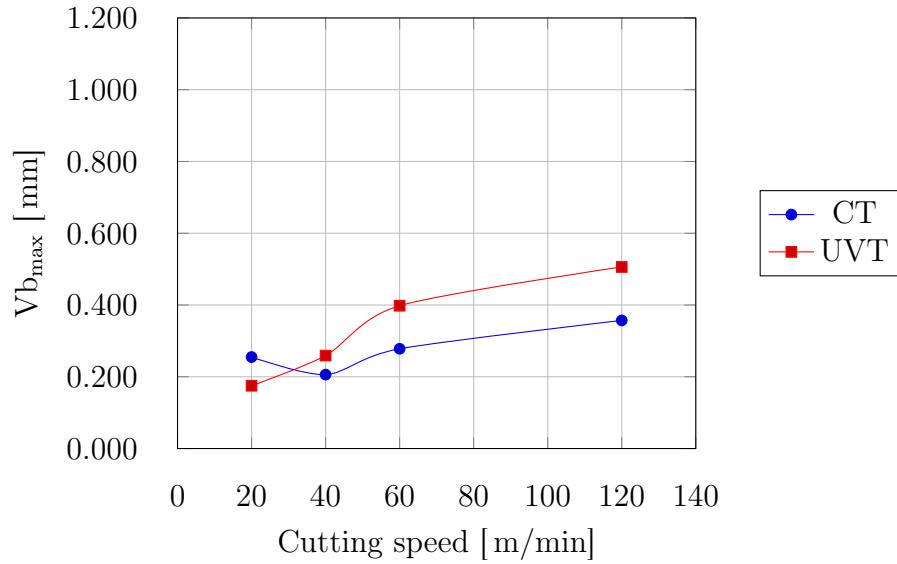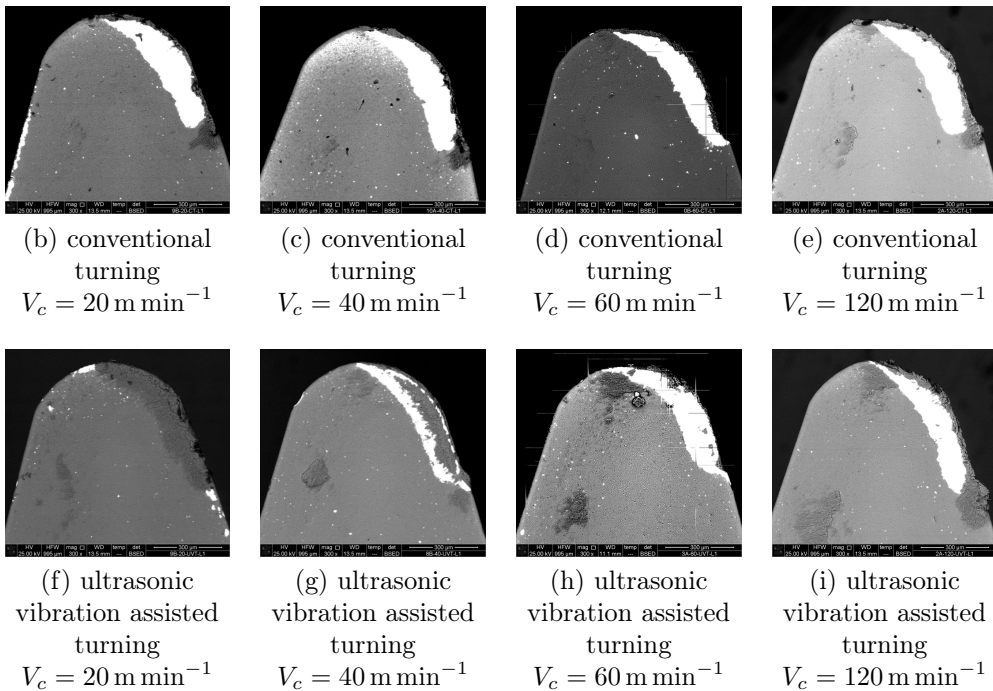
Figure 6.3: Effect of cutting speed at a fixed material removal of $MR = 220\,\mathrm{mm}^3$ and feed of $f = 0{,}06\,\mathrm{mm\,rev}^{-1}$
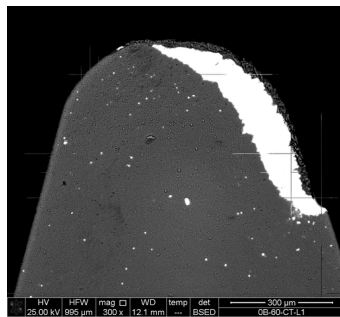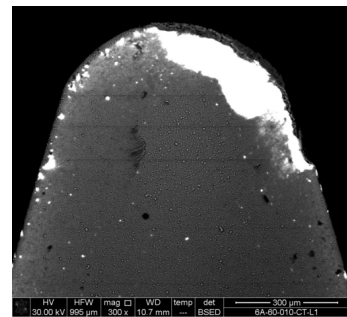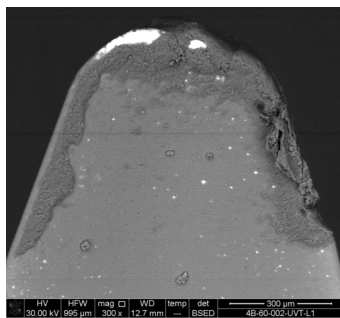
(a) flank wear in function of cutting speed

(b) conventional turning $V_c = 20 \, \text{m} \, \text{min}^{-1}$

(c) conventional turning $V_c = 40 \, \text{m} \, \text{min}^{-1}$

(d) conventional turning $V_c = 60 \, \text{m} \, \text{min}^{-1}$

(e) conventional turning $V_c = 120 \, \text{m} \, \text{min}^{-1}$

(f) ultrasonic vibration assisted turning $V_c = 20 \, \text{m} \, \text{min}^{-1}$

(g) ultrasonic vibration assisted turning $V_c = 40 \, \text{m} \, \text{min}^{-1}$

(h) ultrasonic vibration assisted turning $V_c = 60 \, \text{m} \, \text{min}^{-1}$

(i) ultrasonic vibration assisted turning $V_c = 120 \, \text{m} \, \text{min}^{-1}$

Figure 6.4: Effect of cutting speed at a fixed material removal of $MR = 660 \, \text{mm}^3$ and feed of $f = 0{,}06 \, \text{mm} \, \text{rev}^{-1}$
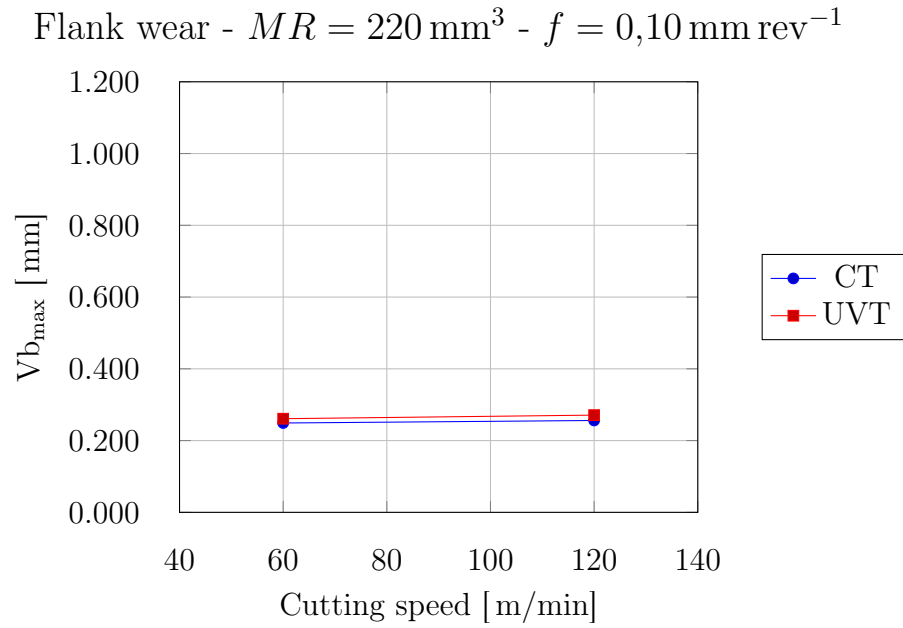
Flank wear - $MR = 220\,\mathrm{mm}^3$ - $f = 0{,}10\,\mathrm{mm\,rev}^{-1}$

(a) flank wear in function of cutting speed
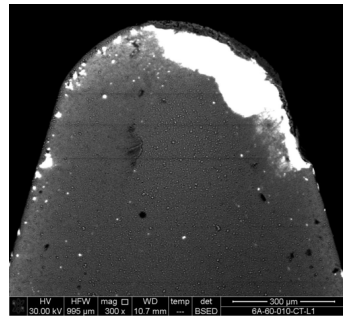
(b) conventional turning
$V_c = 60\,\mathrm{m\,min}^{-1}$

(c) conventional turning
$V_c = 120\,\mathrm{m\,min}^{-1}$

(d) ultrasonic vibration
assisted turning
$V_c = 60\,\mathrm{m\,min}^{-1}$

(e) ultrasonic vibration
assisted turning
$V_c = 120\,\mathrm{m\,min}^{-1}$

Figure 6.5: Effect of cutting speed at a fixed material removal of $MR = 220\,\mathrm{mm}^3$ and feed of $f = 0{,}10\,\mathrm{mm\,rev}^{-1}$

Flank wear - $MR = 660\,\mathrm{mm}^3$ - $f = 0{,}10\,\mathrm{mm\,rev}^{-1}$

(a) flank wear in function of cutting speed

(b) conventional turning
$V_c = 60\,\mathrm{m\,min}^{-1}$

(c) conventional turning
$V_c = 120\,\mathrm{m\,min}^{-1}$

(d) ultrasonic vibration
assisted turning
$V_c = 60\,\mathrm{m\,min}^{-1}$

(e) ultrasonic vibration
assisted turning
$V_c = 120\,\mathrm{m\,min}^{-1}$

Figure 6.6: Effect of cutting speed at a fixed material removal of $MR = 660\,\mathrm{mm}^3$ and feed of $f = 0{,}10\,\mathrm{mm\,rev}^{-1}$

Flank wear - $MR = 220\,\mathrm{mm}^3$ - $V_c = 60\,\mathrm{m\,min}^{-1}$
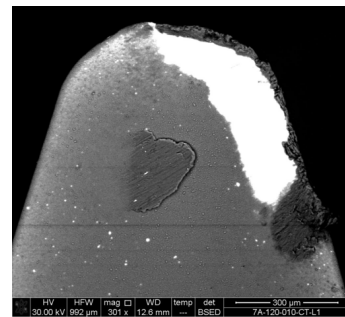

(a) flank wear in function of feed

(b) conventional turning
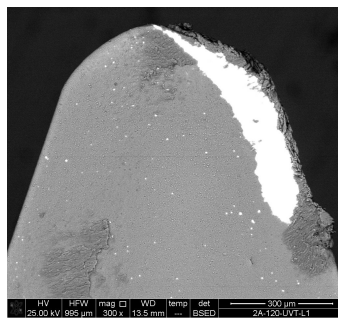$f = 0{,}02\,\mathrm{mm\,rev}^{-1}$

(c) conventional turning
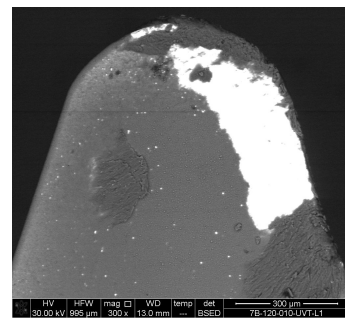$f = 0{,}06\,\mathrm{mm\,rev}^{-1}$

(d) conventional turning
$f = 0{,}10\,\mathrm{mm\,rev}^{-1}$

(e) ultrasonic vibration
assisted turning
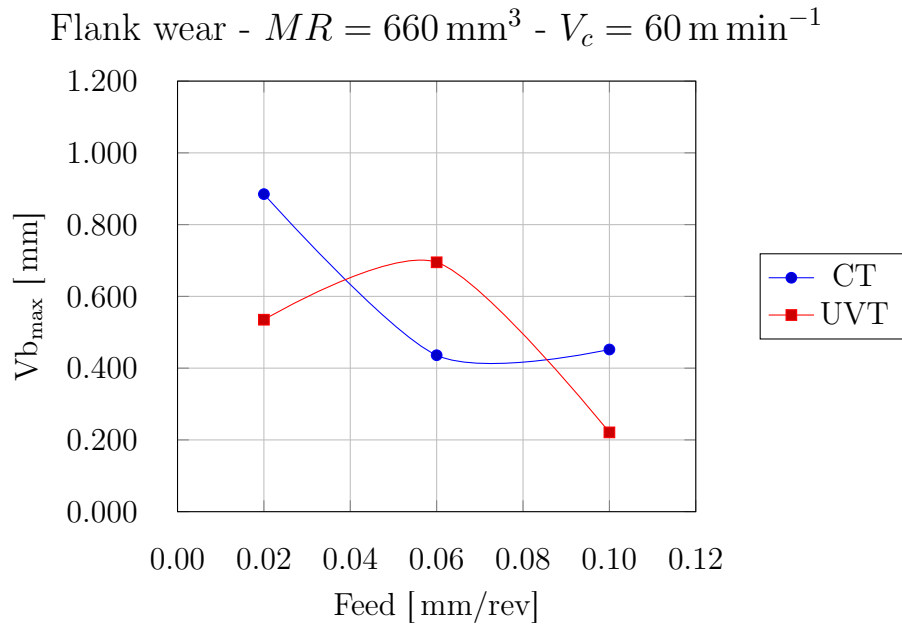$f = 0{,}02\,\mathrm{mm\,rev}^{-1}$
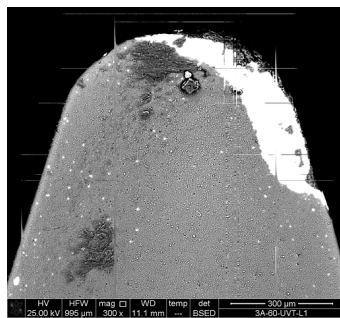
(f) ultrasonic vibration
assisted turning
$f = 0{,}06\,\mathrm{mm\,rev}^{-1}$
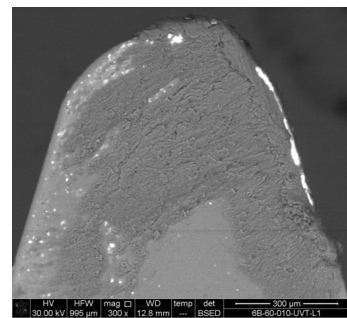
(g) ultrasonic vibration
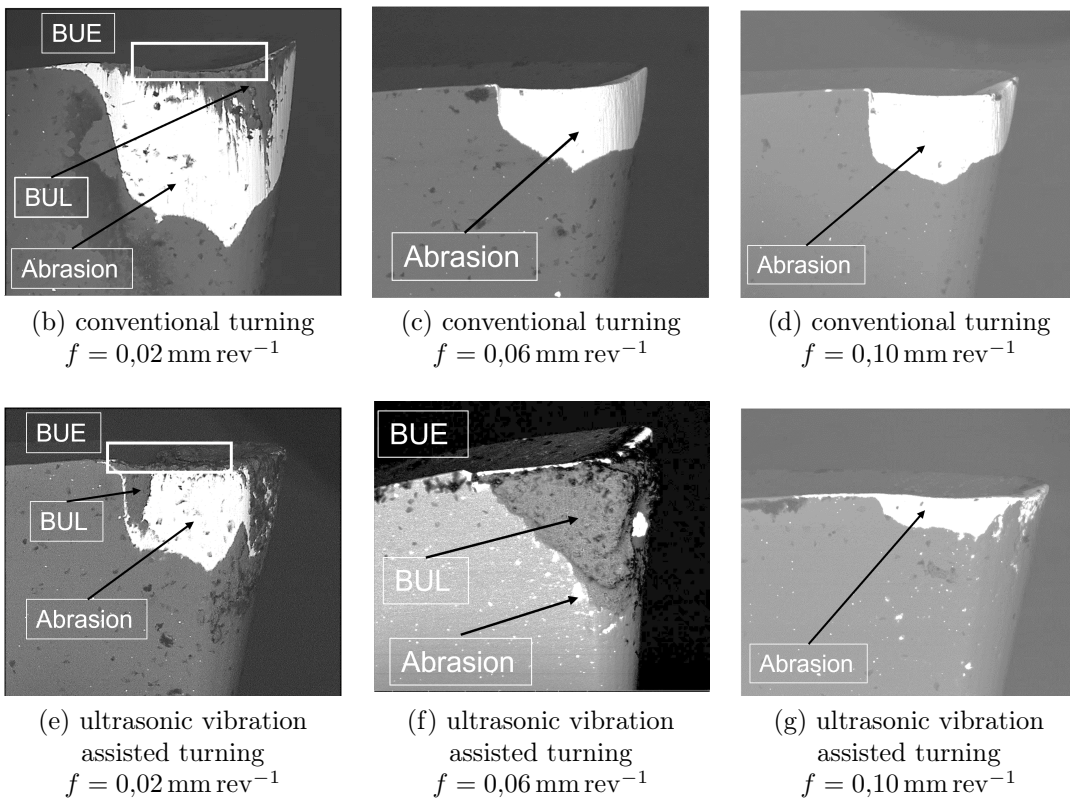assisted turning
$f = 0{,}10\,\mathrm{mm\,rev}^{-1}$

Figure 6.7: Effect of ultrasonic vibration assisted turning at a fixed material removal of $MR = 220\,\mathrm{mm}^3$ and cutting speed of $V_c = 60\,\mathrm{m\,min}^{-1}$

Flank wear - $MR = 220\,\text{mm}^3$ - $V_c = 120\,\text{m}\,\text{min}^{-1}$
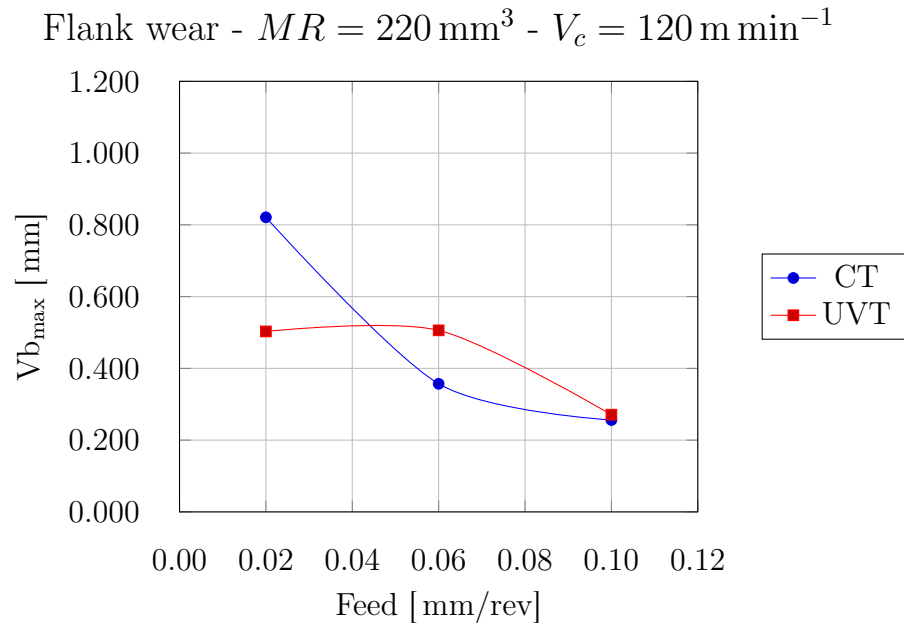
(a) flank wear in function of feed
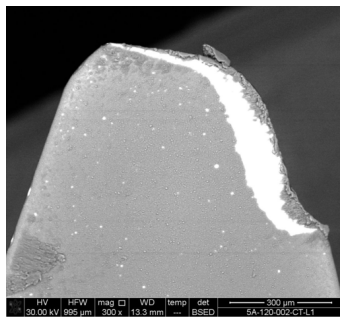
(b) conventional turning
$f = 0{,}02\,\text{mm}\,\text{rev}^{-1}$
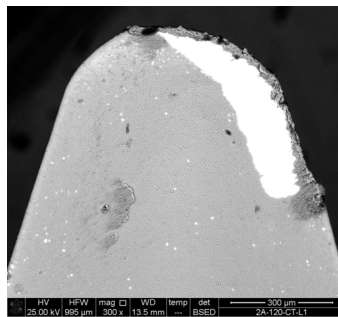
(c) conventional turning
$f = 0{,}06\,\text{mm}\,\text{rev}^{-1}$

(d) conventional turning
$f = 0{,}10\,\text{mm}\,\text{rev}^{-1}$
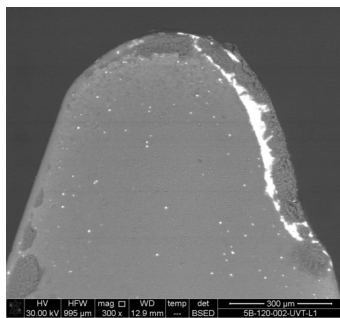
(e) ultrasonic vibration
assisted turning
$f = 0{,}02\,\text{mm}\,\text{rev}^{-1}$

(f) ultrasonic vibration
assisted turning
$f = 0{,}06\,\text{mm}\,\text{rev}^{-1}$

(g) ultrasonic vibration
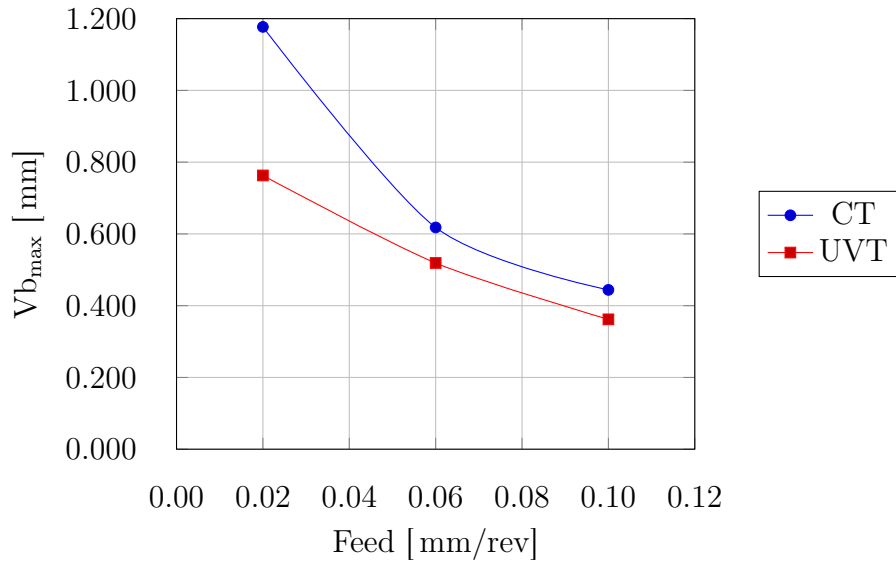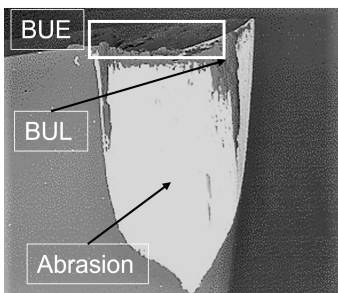assisted turning
$f = 0{,}10\,\text{mm}\,\text{rev}^{-1}$

Figure 6.8: Effect of ultrasonic vibration assisted turning at a fixed material removal of $MR = 220\,\text{mm}^3$ and cutting speed of $V_c = 120\,\text{m}\,\text{min}^{-1}$

Flank wear - $MR = 660 \, \text{mm}^3$ - $V_c = 60 \, \text{m} \, \text{min}^{-1}$

(a) flank wear in function of feed

(b) conventional turning
$f = 0{,}02 \, \text{mm} \, \text{rev}^{-1}$

(c) conventional turning
$f = 0{,}06 \, \text{mm} \, \text{rev}^{-1}$

(d) conventional turning
$f = 0{,}10 \, \text{mm} \, \text{rev}^{-1}$

(e) ultrasonic vibration
assisted turning
$f = 0{,}02 \, \text{mm} \, \text{rev}^{-1}$

(f) ultrasonic vibration
assisted turning
$f = 0{,}06 \, \text{mm} \, \text{rev}^{-1}$

(g) ultrasonic vibration
assisted turning
$f = 0{,}10 \, \text{mm} \, \text{rev}^{-1}$

Figure 6.9: Effect of ultrasonic vibration assisted turning at a fixed material removal of $MR = 660 \, \text{mm}^3$ and cutting speed of $V_c = 60 \, \text{m} \, \text{min}^{-1}$

Flank wear - $MR = 660\,\mathrm{mm}^3$ - $V_c = 120\,\mathrm{m\,min}^{-1}$
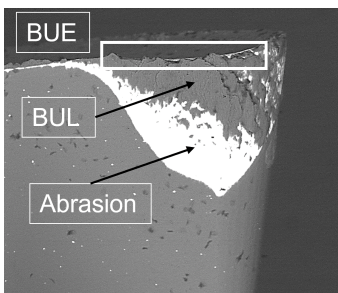

(a) flank wear in function of feed
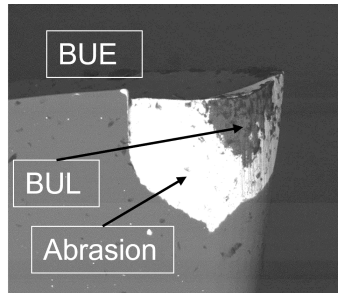
(b) conventional turning
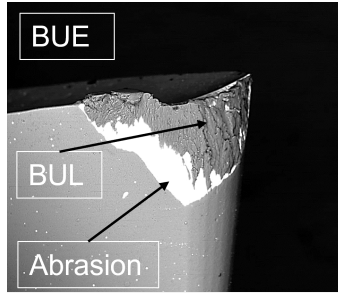$f = 0{,}02\,\mathrm{mm\,rev}^{-1}$

(c) conventional turning
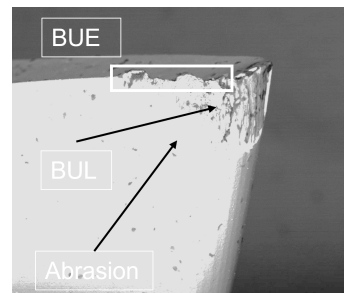$f = 0{,}06\,\mathrm{mm\,rev}^{-1}$
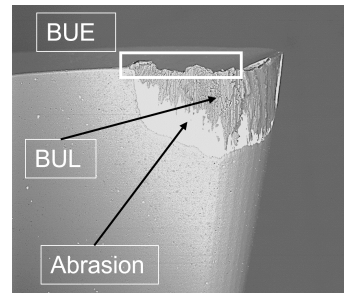
(d) conventional turning
$f = 0{,}10\,\mathrm{mm\,rev}^{-1}$

(e) ultrasonic vibration
assisted turning
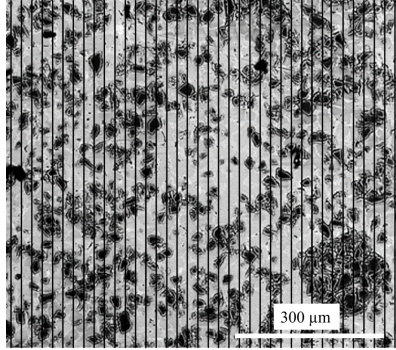$f = 0{,}02\,\mathrm{mm\,rev}^{-1}$

(f) ultrasonic vibration
assisted turning
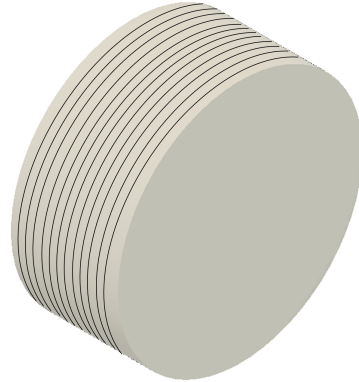$f = 0{,}06\,\mathrm{mm\,rev}^{-1}$

(g) ultrasonic vibration
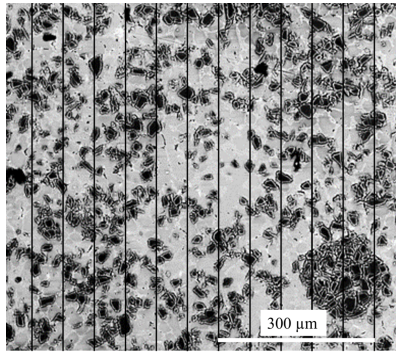assisted turning
$f = 0{,}10\,\mathrm{mm\,rev}^{-1}$

Figure 6.10: Effect of ultrasonic vibration assisted turning at a fixed material removal of $MR = 660\,\mathrm{mm}^3$ and cutting speed of $V_c = 120\,\mathrm{m\,min}^{-1}$
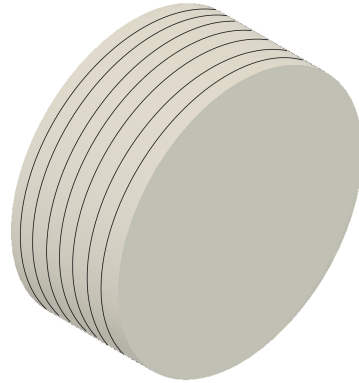
(a) $f = 0{,}02\,\mathrm{mm\,rev^{-1}}$.

(b) Cutting distance at
$f = 0{,}02\,\mathrm{mm\,rev^{-1}}$.

(c) $f = 0{,}06\,\mathrm{mm\,rev^{-1}}$.

(d) Cutting distance at
$f = 0{,}06\,\mathrm{mm\,rev^{-1}}$.
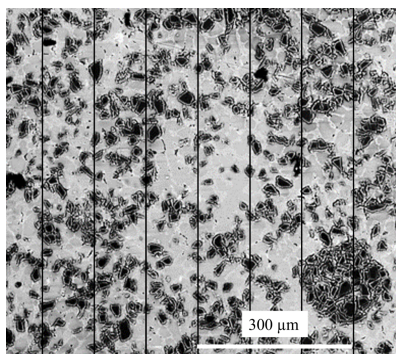
(e) $f = 0{,}10\,\mathrm{mm\,rev^{-1}}$.
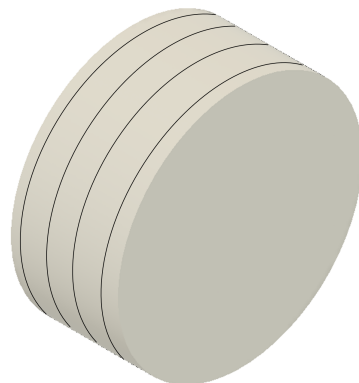
(f) Cutting distance at
$f = 0{,}10\,\mathrm{mm\,rev^{-1}}$.

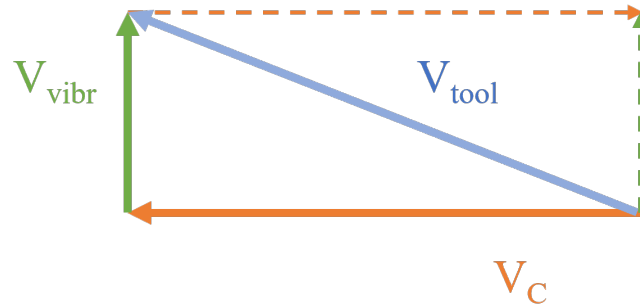Figure 6.11: Hypothetical feed marks on the metal matrix composite

Figure 6.12: Sum of cutting speed and vibrational speed on tool.
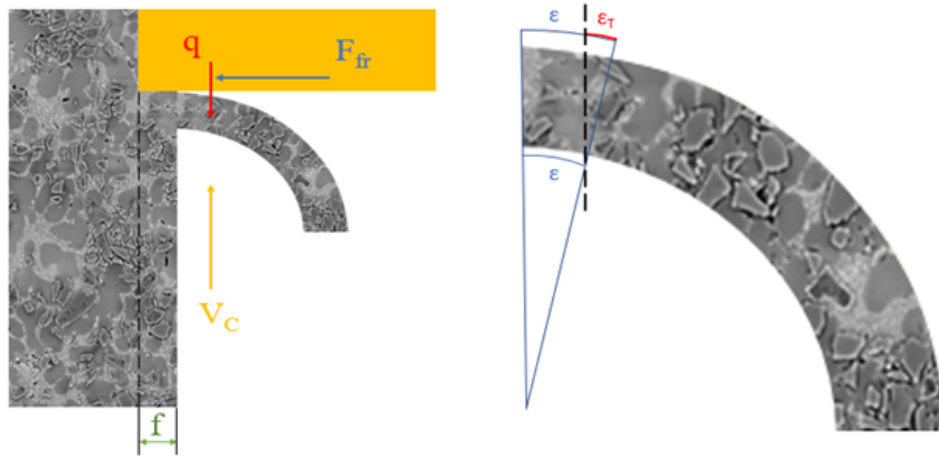
(a) Top view of the chip formation: the friction force is represented with a blue arow: the heat generated by the friction is represented by a red arrow; the cutting speed is represented by a yellow arrow; the tool is schematized with a yellow rectangle.

(b) Detail of deformation: the chip side near the tool has a greater deformation than the opposite side, causing a rotation.

Figure 6.13: Rotation of the chip.

61
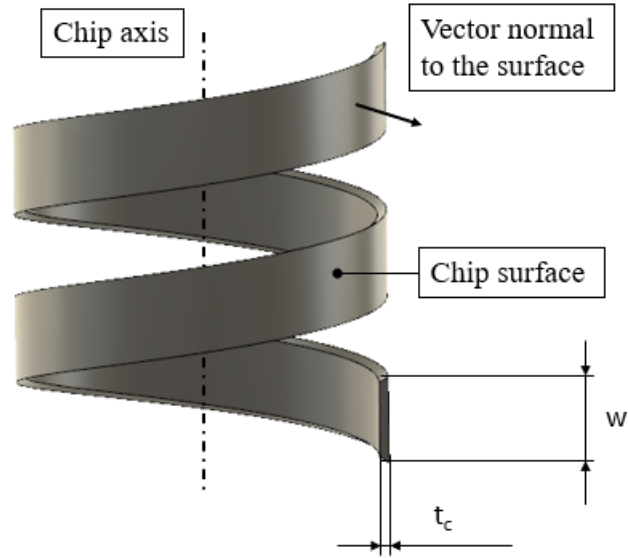
Figure 6.14: Dimensions of the chip.

(a) Tubular chip: Normal of surface (orange) is orthogonal to the chip axis (black)

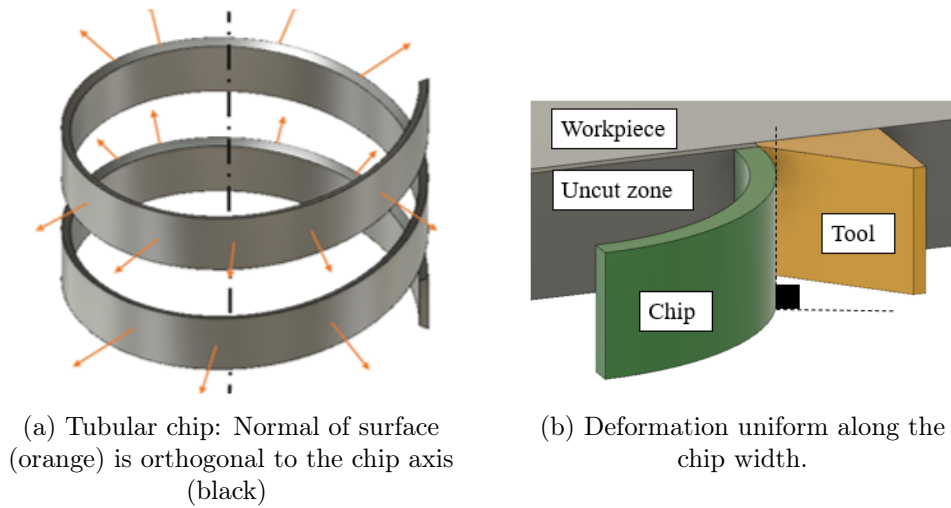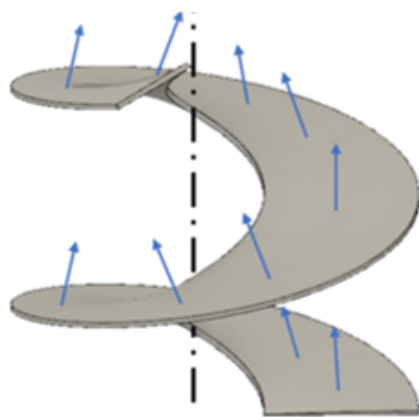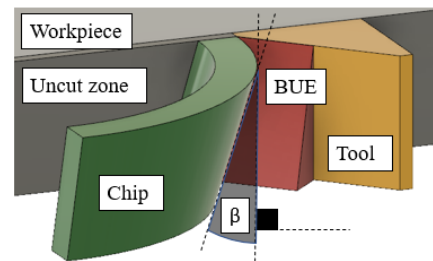(b) Deformation uniform along the chip width.

Figure 6.15: Tubular chip.

(a) Washer-type helical chip: normal of the surface (blue) is parallel to the chip axis (black).

(b) The BUE causes a local deformation which inclines the chip of a β angle.

Figure 6.16: Formation of conical and washer-type chip.

Bibliography

[1]   A. Asgari. "Cutting Conditions Optimisation of Titanium Metal Matrix Composites in Turning and Face Milling." Master thesis. École Polytechnique de Montréal, 2015.

[2]   Wei Bai et al. "Enhanced machinability of SiC-reinforced metal-matrix composite with hybrid turning". In: *Journal of Materials Processing Technology* 268 (2019), pp. 149–161. ISSN: 0924-0136. DOI: `https://doi.org/10.1016/j.jmatprotec.2019.01.017`. URL: `https://www.sciencedirect.com/science/article/pii/S0924013619300238`.

[3]   Jokin Beristain, Oscar Gonzalo, and Alejandro Sandá. "Machinability of Al-SiC metal matrix composites using WC, PCD and MCD inserts". In: *Revista de Metalurgia* 50 (2014). DOI: `10.3989/revmetalm.006`. URL: `https://revistademetalurgia.revistas.csic.es/index.php/revistademetalurgia/article/view/1311`.

[4]   M Mahendra Boopathi, KP Arulshri, and N Iyandurai. "Evaluation of mechanical properties of aluminium alloy 2024 reinforced with silicon carbide and fly ash hybrid metal matrix composites". In: *American journal of applied sciences* 10.3 (2013), p. 219.

[5]   Francois Cardarelli. *Materials Handbook: A Concise Desktop Reference*. Jan. 2008, p. 1339. ISBN: 978-1-84628-668-1. DOI: `10.1007/978-1-84628-669-8`.

[6]   Bill Clyne. "An Introductory Overview of MMC Systems, Types, and Developments". In: *Comprehensive Composite Materials* (Dec. 2000). DOI: `10.1016/B0-08-042993-9/00001-2`.

[7]   J.R. Davis. *Alloying: Understanding the Basics*. ASM International, 2001. ISBN: 9781615030637. URL: `https://books.google.it/books?id=Sg9fAVdf8WoC`.

[8]   M Egilmez et al. "Electrical and mechanical properties of superconducting MgB2/Mg metal matrix composites". In: *Superconductor Science and Technology* 19.4 (2006), p. 359.

[9] M. Geetha et al. "Ti based biomaterials, the ultimate choice for orthopaedic implants – A review". In: *Progress in Materials Science* 54.3 (2009), pp. 397–425. ISSN: 0079-6425. DOI: https://doi.org/10.1016/j.pmatsci.2008.06.004. URL: https://www.sciencedirect.com/science/article/pii/S0079642508001126.

[10] TMT Gofrey, Paul S Goodwin, and C Malcolm Ward-Close. "Titanium particulate metal matrix composites–Reinforcement, production methods, and mechanical properties". In: *Advanced Engineering Materials* 2.3 (2000), pp. 85–91.

[11] Hasan Gokkaya and Ahmet Taşkesen. "The effects of cutting speed and feed rate on BUE-BUL formation, cutting forces and surface roughness when machining AA6351 (T6) alloy". In: *Strojniski Vestnik/Journal of Mechanical Engineering* 54 (Aug. 2008), pp. 521–530.

[12] Aaron Greco et al. "Surface texturing of tribological interfaces using the vibromechanical texturing method". In: *Journal of Manufacturing Science and Engineering* 131.6 (2009), pp. 0610051–0610058. DOI: 10.1115/1.4000418.

[13] M. Haghshenas. *Metal–Matrix Composites*. Elsevier, 2016. ISBN: 978-0-12-803581-8. DOI: https://doi.org/10.1016/B978-0-12-803581-8.03950-3. URL: https://www.sciencedirect.com/science/article/pii/B9780128035818039503.

[14] Xiao Han et al. "On understanding the specific cutting mechanisms governing the workpiece surface integrity in metal matrix composites machining". In: *Journal of Materials Processing Technology* 288 (2021), p. 116875. ISSN: 0924-0136. DOI: https://doi.org/10.1016/j.jmatprotec.2020.116875. URL: https://www.sciencedirect.com/science/article/pii/S0924013620302892.

[15] Changshu He et al. "Coupling effect of axial ultrasonic vibration and tool thread on the microstructure and properties of the friction stir lap welding joint of Al/Mg dissimilar alloys". In: *Journal of Manufacturing Processes* 80 (2022), pp. 95–107. ISSN: 1526-6125. DOI: https://doi.org/10.1016/j.jmapro.2022.05.008. URL: https://www.sciencedirect.com/science/article/pii/S152661252200322X.

[16] D Jani. "Machining of Sic—metal matrix composite (MMC) by polycrystalline diamond (PCD) tools and effect on quality of surface by changing machining parameters". In: *Int. J. Sci. Res. Dev* 2 (2014), pp. 106–108.

[17] J.R. Johnston et al. *Performance of Rocket Nozzle Materials with Several Solid Propellants*. NASA technical note v. 3428. National Aeronautics and Space Administration, 1966. URL: https://books.google.it/books?id=emsPpywqChEC.

[18] S. Kalpakjian and S.R. Schmid. *Manufacturing Engineering and Technology*. Pearson, 2014. ISBN: 9780133128741. URL: `https://books.google.it/books?id=frF9MgEACAAJ`.

[19] Zhirong Liao et al. "State-of-the-art of surface integrity in machining of metal matrix composites". In: *International Journal of Machine Tools and Manufacture* 143 (2019), pp. 63–91. ISSN: 0890-6955. DOI: `https://doi.org/10.1016/j.ijmachtools.2019.05.006`. URL: `https://www.sciencedirect.com/science/article/pii/S0890695519301889`.

[20] Natarajan Nanjappan et al. "Dry Sliding Wear and Mechanical Behavior of Aluminium/Fly ash/Graphite Hybrid Metal Matrix Composite Using Taguchi Method". In: *Int. J. Modern. Eng. Res.* 23 (Jan. 2012), pp. 2249–6645.

[21] Amal E Nassar and Eman E Nassar. "Properties of aluminum matrix Nano composites prepared by powder metallurgy processing". In: *Journal of king saud university-Engineering sciences* 29.3 (2017), pp. 295–299.

[22] Y Sahin. "Wear behaviour of aluminium alloy and its composites reinforced by SiC particles using statistical analysis". In: *Materials & design* 24.2 (2003), pp. 95–103.

[23] Pranav Dev Srivyas and MS Charoo. "Role of reinforcements on the mechanical and tribological behavior of aluminum metal matrix composites–a review". In: *Materials Today: Proceedings* 5.9 (2018), pp. 20041–20053.

[24] ISO: International Organization for Standardization. *Tool-life testing with single-point turning tools*. 1993.

[25] M. K. Surappa. "Aluminium matrix composites: Challenges and opportunities". In: *Sadhana* 28.1 (Feb. 2003), pp. 319–334. ISSN: 0973-7677. DOI: `10.1007/BF02717141`. URL: `https://doi.org/10.1007/BF02717141`.

Appendix A

MATLAB code for the computing of percentage of silicon carbide particles

This program analyses the images taken by the stereo microscope after the etching of the samples, as explained in 4. In particular, it computes the percentage of silicon carbide particles in the images. For this program it's necessary to have at least one image in the same directory of this program. The images taken were all *Tagged Image Files* (.tif) but can be used also other types of graphic files. For further explainations, see the MATLAB documentation. In the first instance, the image is read from the *imread* function, then saved as a matrix called *I* which size depends on the original sizes of the image. The same image is saved also in another matrix *I_or*.[1] The image will be transformed in a grayscale image with the function *rgb2gray*. The image is shown to verify that the conversion is made in the right way. It's noticed that the grayscale image is similar to the original image, as shown in A.1 because the stereo microscope didn't colour the pictures as explained in 4. In these images can be distinguished three levels of gray: the white, which is recognizable as aluminium; the big dark gray particles,which are recognizable as silicon carbide, and the light gray particles which are recognizable as alloy precipitates. So, a filtering is necessary in order to remove the precipitates parts form the image. To do so, a mask must be built. Two values of gray, stored in *gray1* and *gray2* must be chosen to get the range of values which corresponds to the silicon carbide particles. Then a mask can be built, taking all the pixes which are in the range given by the two values. *gray1* and *gray2* must have a value from 0 (black) to 255 (white).

---

[1] From this point to the end of this program the images are taken as matrix and the pixels are taken as elements of the matrix.

After that, all the pixels which are not in the mask are transformed in white pixels by the function *I(∼mask)*. Doing that, all the light gray and dark gray pixel are gone, leaving only the silicon carbide particles pixels. Then a montage between the original image and the filtered image is made to check if there are some silicon carbide particles which are missing. An example of montage is shown in A.2. If some of them are missing, the values of *gray1* and *gray2* must be changed.

Then, to transform all the dark grey pixels to black pixels, another transformation is needed: the image must be transform in black and white. To do so, the function *imbinarize* is used to transform the image from grayscale filtered to black and white. To use the function *imbinarize* is needed a threshold value which is computed with the function *graythresh*.

Another montage is done to check if the transformation is correct. An example of montage is shown in A.3. At this point, there is a image with only black and white pixels, so it's used the function *numel* to compute the total number of pixels in the image stored in the variable *tot*, and the function *nnz* to compute the number of white pixels stored in the variable *white*, from which can be computed the percentage of black pixels. A simpified formula is used:

$$\%_{SiC} = 100\frac{N_{black}}{N_{tot}} = 100\frac{N_{tot} - N_{white}}{N_{tot}} = 100\frac{1 - N_{white}}{N_{tot}} \tag{A.1}$$

```matlab
1  % read the image
2  I = imread('nameimage.extension');
3  I_or = I;
4
5  % trasform the image from RGB to grayscale
6  I = rgb2gray(I);
7
8  % shows the new grayscale image
9  figure(1)
10 imshow(I);
11 hold off;
12
13 % mask to filter the gray parts which are silicon carbide
14 % the values of gray3 and gray4 must be adjusted
15 % for every image to permit a good filtering
16 % range of gray3 and gray4 is from 0 to 255
17 gray1 = 90;
18 gray2 = 170;
19 mask = I >= gray3 & I <= gray4;
20 I(~mask) = 255;
21 % montage of the images before and after the filtering
22 figure(2)
23 imshowpair(I_or,I,'montage');
24 hold off;
25
26 % trasform the image from grayscale to black and white
27 level = graythresh(I);
28 BW = imbinarize(I,level);
29
30 % shows the new black and white image
31 figure(3)
32 imshowpair(I,BW,'montage');
33
34 % computes the % of carbides counting the number
35 % of black pixels in respect of all pixels
36 tot = numel(BW);
37 white = nnz(BW);
38 perc = 100*(1-white/tot);
39 fprintf('Threshold: %.2f \n',level);
40 fprintf('Percentage of carbides: %.2f \n',perc);
```
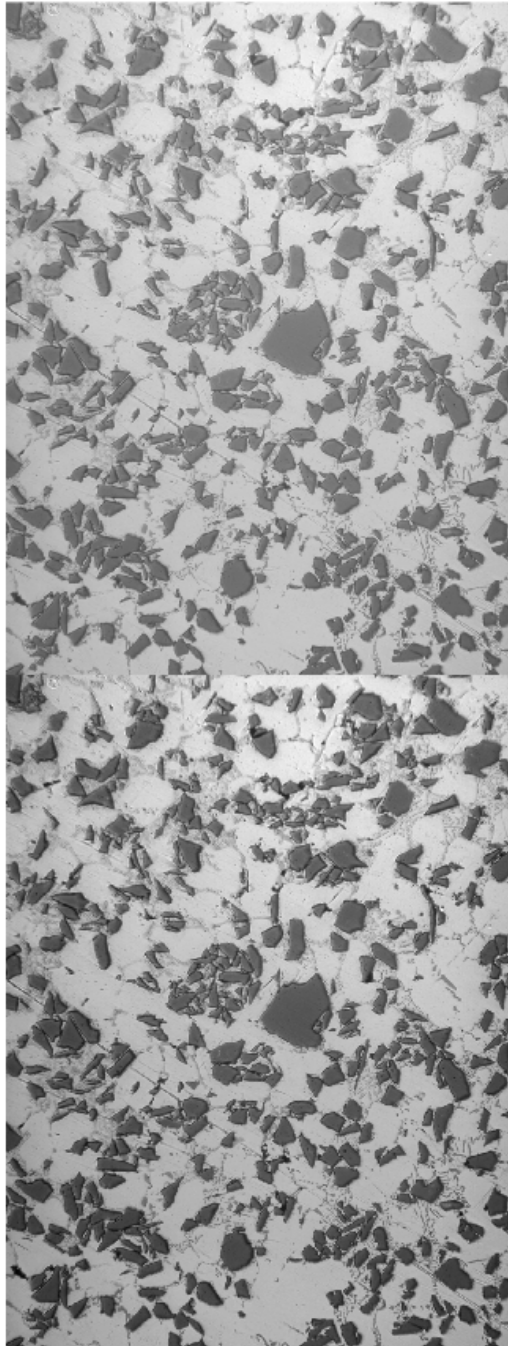
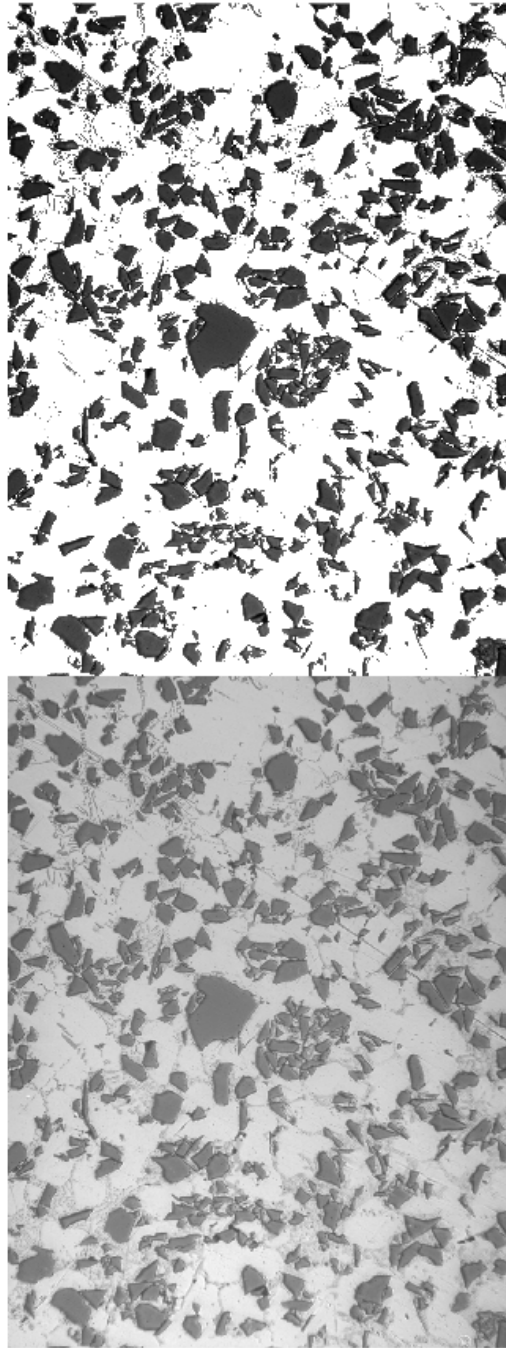Figure A.1: Transformation from original image to grayscale image

Figure A.2: Transformation from grayscale image to filtered grayscale image
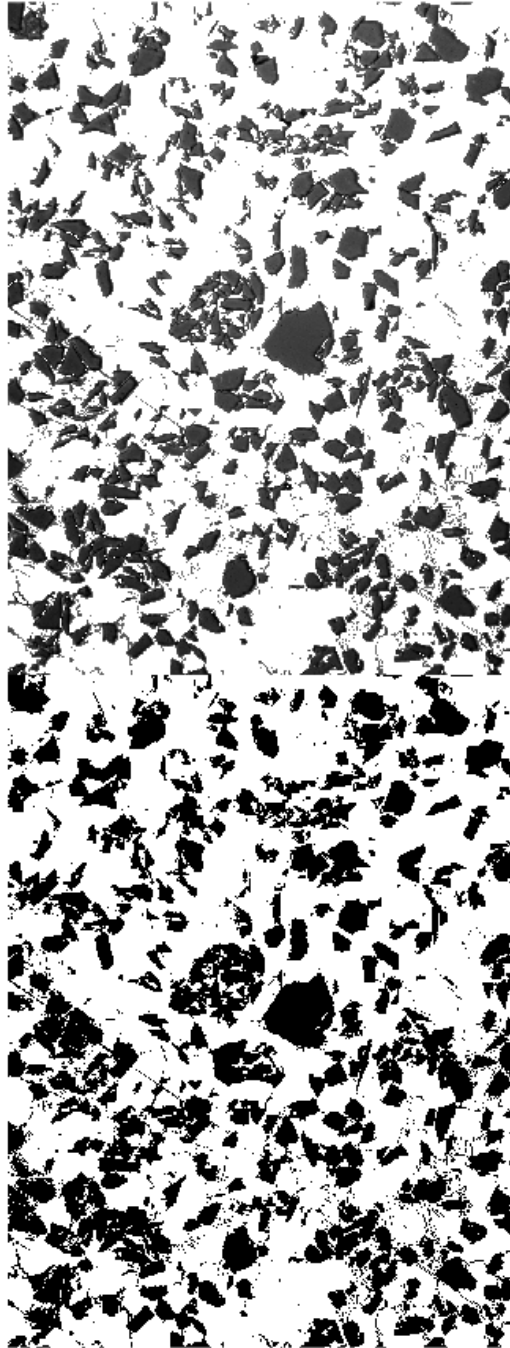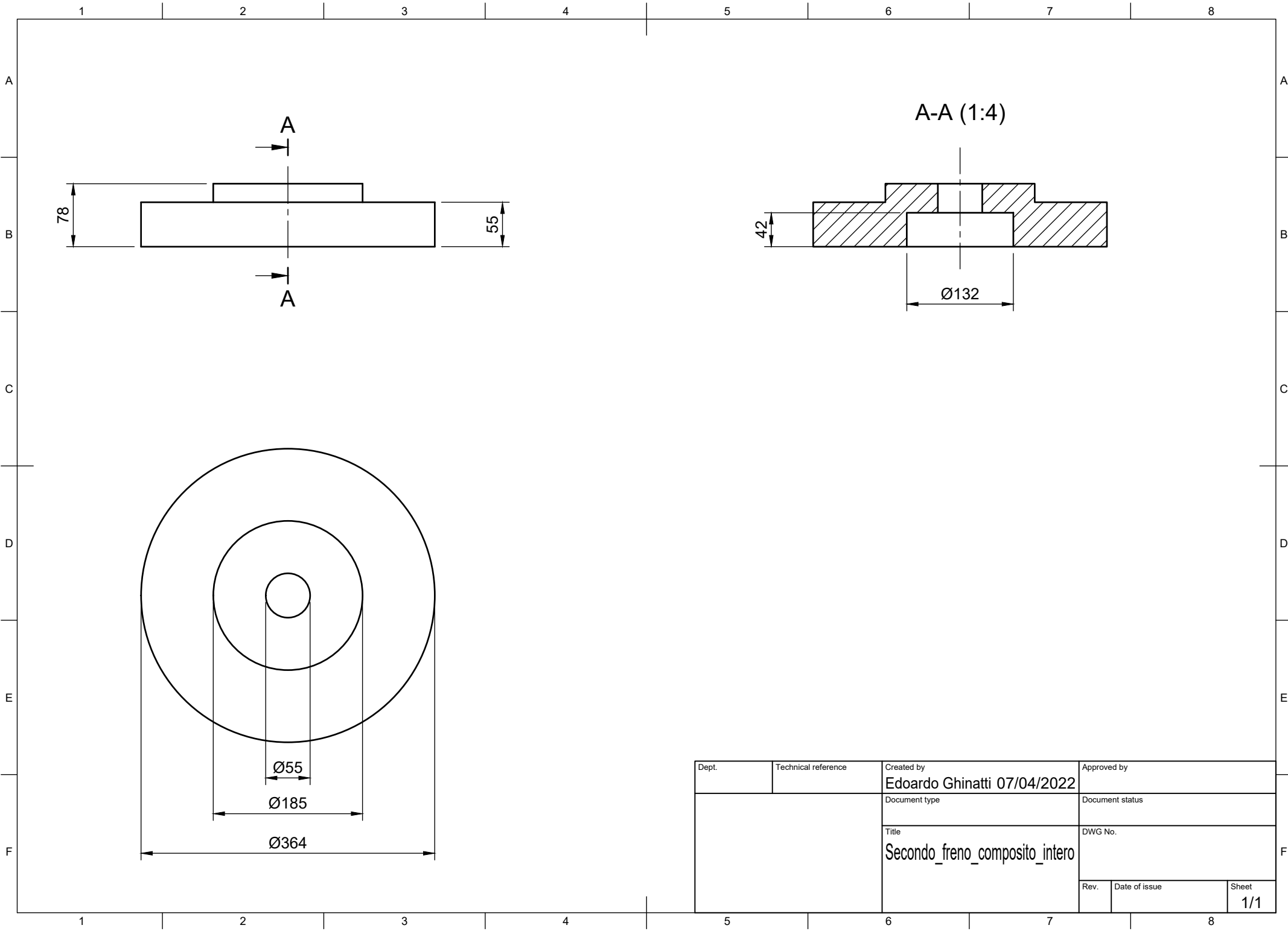
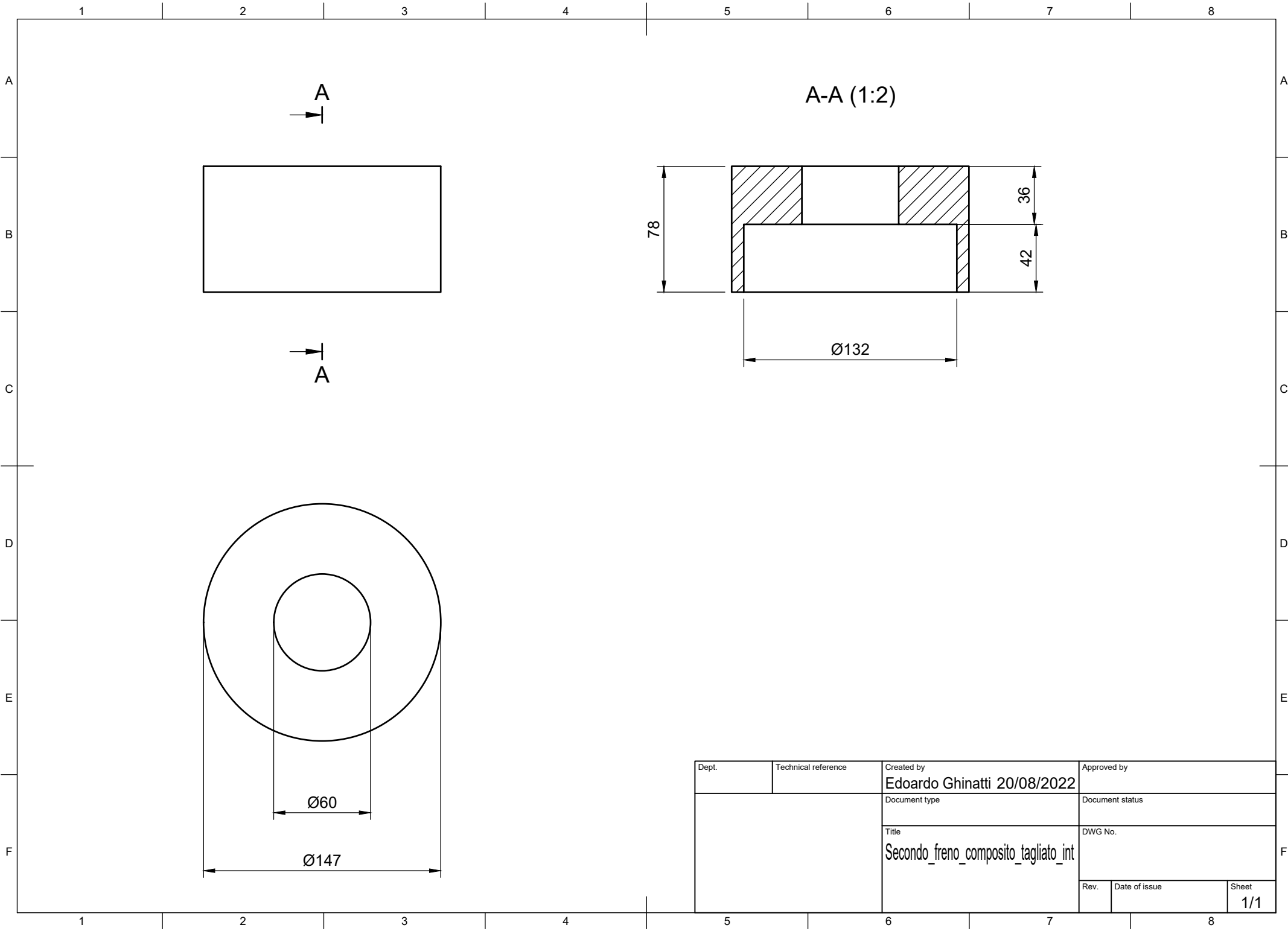Figure A.3: Transformation from filtered grayscale image to black and white image
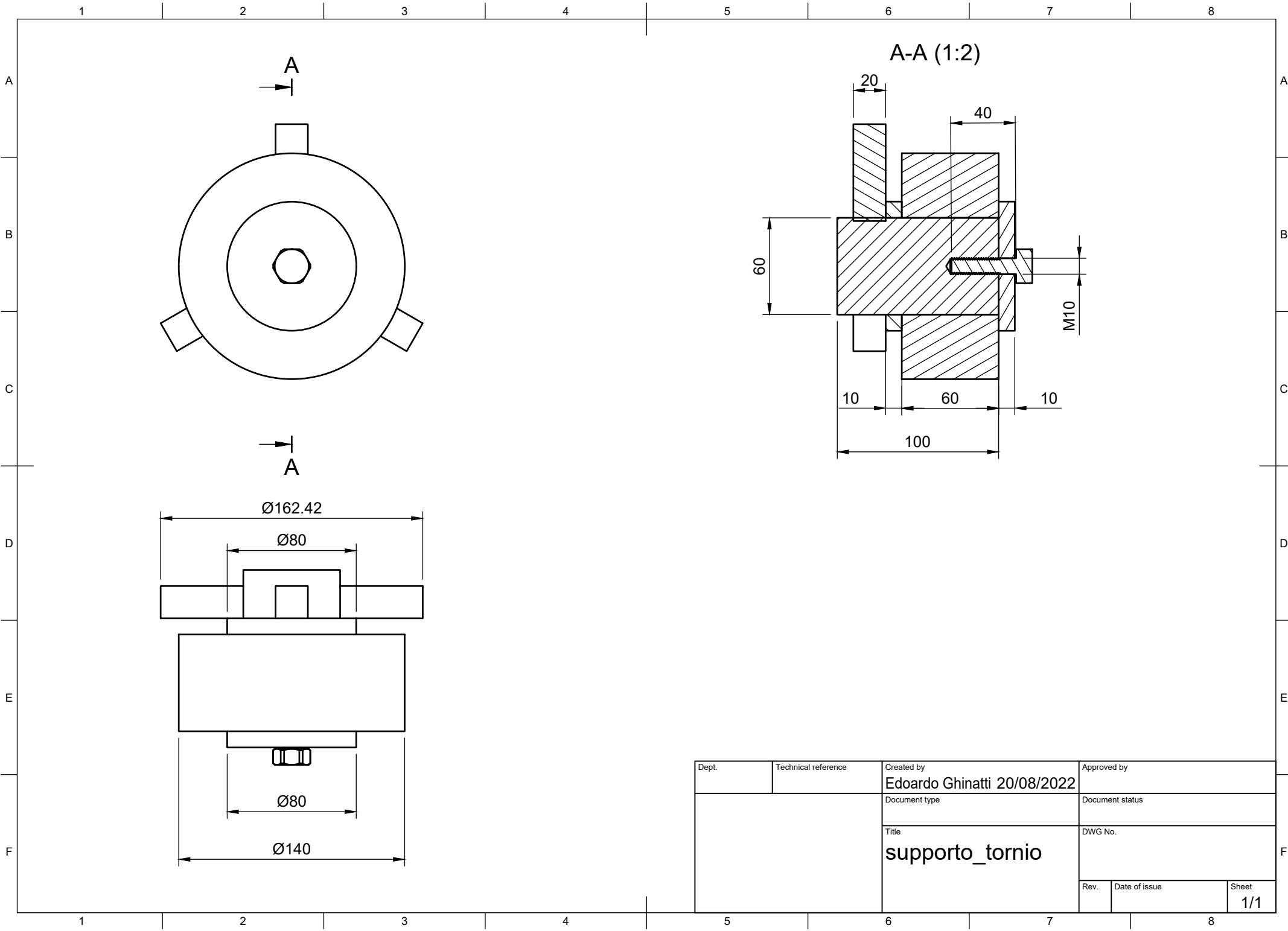
Appendix B

Drawings

In this appendix are presented all the drawings used for this thesis: the first drawing is the original disc brake, the second one is the brake disc after the water-jet cut, which was necessary to to make it compatible with the lathe cutting limits, and the third drawing is the support necessary for the disc machining.

A

A-A (1:4)

78

55

A

42

Ø132

Ø55

Ø185

Ø364

A-A (1:2)

78

36

42

Ø132

A

A

Ø60

Ø147

A

A-A (1:2)

20
40
60
M10
10
60
10
100

A

Ø162.42
Ø80

Ø80
Ø140

Dept.	Technical reference	Created by	Approved by	
		Edoardo Ghinatti 20/08/2022		
		Document type	Document status	
		Title	DWG No.	
		supporto_tornio		
			Rev.	Date of issue	Sheet 1/1